

Chapter 1

THEORY OF MANGANITES

Takashi HOTTA¹ and Elbio DAGOTTO²

¹Advanced Science Research Center
Japan Atomic Energy Research Institute
Tokai, Ibaraki 319-1195, JAPAN

²National High Magnetic Field Laboratory
Florida State University
Tallahassee, FL32310, U.S.A.

In this review, the present status of theories for manganites is discussed. The complex phase diagrams of these materials, with a variety of spin-charge-orbital ordering tendencies, is addressed using mean-field and Monte Carlo simulation techniques. The stability of the charge-ordered states, such as the CE-state at half-doping, appears to originate, in part, in the topology of the zigzag chains present in those states. In addition, it is argued that phase separation tendencies are notorious in realistic models for Mn-oxides. They produce nanoscale clusters of competing phases, either through an electronic separation tendency or through the influence of disorder on first-order transitions. These inhomogeneities lead to a “colossal” magnetoresistance (CMR) effect, compatible with experiments. This brief review is based on a more extensive work recently presented [E. Dagotto, T. Hotta, and A. Moreo, *Phys. Rep.* **344**, 1 (2001)]. There, a comprehensive analysis of the experimental literature can be found. In real manganites, the tendencies toward inhomogeneous states are notorious in CMR regimes, in excellent agreement with the theoretical description outlined here.

1. Early Theoretical Studies of Manganites

Most of the early theoretical work on manganites focused on the qualitative aspects of the experimentally discovered relation between transport and magnetic properties, namely the increase in conductivity upon the polarization of the spins. Not much work was devoted to the magnitude of the magnetoresistance effect itself. The formation of coexisting clusters of competing phases was not included in the early considerations, but this is the dominant theory at present. The states of manganites were assumed to be uniform, and “Double Exchange” (DE) was proposed by Zener (1951) as a way to allow for charge to move in manganites by the generation of a spin polarized state. The DE process has been historically explained in two somewhat different ways. Originally, Zener (1951) considered the explicit movement of electrons schematically written as $\text{Mn}_{1\uparrow}^{3+}\text{O}_{2\uparrow,3\downarrow}\text{Mn}^{4+} \rightarrow \text{Mn}^{4+}\text{O}_{1\uparrow,3\downarrow}\text{Mn}_{2\uparrow}^{3+}$ where 1, 2, and 3 label electrons that belong either to the oxygen between manganese, or to the e_g -level of the Mn-ions. In this process there are two *simultaneous* motions (thus the name double-exchange) involving electron 2 moving from the oxygen to the right Mn-ion, and electron 1 from the left Mn-ion to the oxygen. The second way to visualize DE processes was presented in detail by Anderson and Hasegawa (1955) and it involves a second-order process in which the two states described above go from one to the other using an intermediate state $\text{Mn}_{1\uparrow}^{3+}\text{O}_{3\downarrow}\text{Mn}_{2\uparrow}^{3+}$. In this context the effective hopping for the electron to move from one Mn-site to the next is proportional to the square of the hopping involving the p -oxygen and d -manganese orbitals (t_{pd}). In addition, if the localized spins are considered classical and with an angle θ between nearest-neighbor ones, the effective hopping becomes proportional to $\cos(\theta/2)$, as shown by Anderson and Hasegawa (1955). If $\theta=0$ the hopping is the largest, while if $\theta=\pi$, corresponding to an antiferromagnetic background, then the hopping cancels.

Note that the oxygen linking the Mn-ions is crucial to understand the origin of the word “double” in this process. Nevertheless, the majority of the theoretical work carried out in the context of manganites simply forgets the presence of the oxygen and uses a manganese-only Hamiltonian. It is interesting to observe that ferromagnetic states appear in this context even *without* the oxygen. It is clear that the electrons simply need a polarized background to improve their kinetic energy, in similar ways as the Nagaoka phase is generated in the one-band Hubbard model at large U/t (for a high- T_c review, see Dagotto, 1994). This tendency to optimize the kinetic energy is at work in a variety of models and the term double-exchange appears unnecessary. However, in spite of this fact it has become customary to refer to virtually any ferromagnetic phase found in manganese models as “DE induced” or “DE generated”,

forgetting the historical origin of the term. In this review a similar convention will be followed, namely the credit for the appearance of FM phases will be given to the DE mechanism, although a more general and simple kinetic-energy optimization is certainly at work.

Regarding the stabilization of ferromagnetism, computer simulations (Yunoki et al., 1998a) and a variety of other approximations have clearly shown that models *without* the oxygen degrees of freedom (to be reviewed below) can also produce FM phases, as long as the Hund coupling is large enough. In this situation, when the e_g electrons directly jump from Mn to Mn their kinetic energy is minimized if all spins are aligned. As explained before, this procedure to obtain ferromagnetism is usually also called double-exchange and even the models from where it emerges are called double-exchange models.

At this point it is useful to discuss the well-known proposed “spin canted” state for manganites. Work by de Gennes (1960) using mean-field approximations suggested that the interpolation between the antiferromagnetic state of the undoped limit and the ferromagnetic state at finite hole density, where the DE mechanism works, occurs through a “canted state”, similar as the state produced by a magnetic field acting over an antiferromagnet. In this state the spins develop a moment in one direction, while being mostly antiparallel within the plane perpendicular to that moment. The coexistence of FM and AF features in several experiments carried out at low hole doping (some of them reviewed below) led to the widely spread belief, until recently, that this spin canted state was indeed found in real materials. However, a plethora of recent theoretical work (also discussed below) has shown that the canted state is actually not realized in the model of manganites studied by de Gennes (i.e., the simple one-orbital model). Instead phase separation occurs between the AF and FM states, as extensively reviewed below. Nevertheless, a spin canted state is certainly still a possibility in real low-doped manganites but its origin, if their presence is confirmed, needs to be revised. It may occur that substantial Dzyaloshinskii-Moriya (DM) interactions appear in manganese oxides, but the authors are not aware of experimental papers confirming or denying their relevance.

Early theoretical work on manganites carried out by Goodenough (1955) explained many of the features observed in the neutron scattering $\text{La}_{1-x}\text{Ca}_x\text{MnO}_3$ experiments by Wollan and Koehler (1955), notably the appearance of the A-type AF phase at $x=0$ and the CE-type phase at $x=0.5$. The approach of Goodenough (1955) was based on the notion of “semicovalent exchange”. Analyzing the various possibilities for the orbital directions and generalizing to the case where Mn^{4+} ions are also present, Goodenough (1955) arrived to the A- and CE-type phases of

manganites very early in the theoretical study of these compounds. In this line of reasoning, note that the Coulomb interactions are important to generate Hund-like rules and the oxygen is also important to produce the covalent bonds. The lattice distortions are also quite relevant in deciding which of the many possible states minimizes the energy. However, it is interesting to observe that in more recent theoretical work described below in this review, both the A- and CE-type phases can be generated without the explicit appearance of oxygens in the models and also without including long-range Coulombic terms.

Summarizing, there appears to be three mechanisms to produce effective FM interactions: (i) double exchange, where electrons are mobile, which is valid for non charge-ordered states and where the oxygen plays a key role, (ii) Goodenough's approach where covalent bonds are important (here the electrons do not have mobility in spite of the FM effective coupling), and it mainly applies to charge-ordered states, and (iii) the approach based on purely Mn models (no oxygens) which leads to FM interactions mainly as a consequence of the large Hund coupling in the system. If phonons are introduced in the model it can be shown that the A-type and CE-type states are generated. In the remaining theoretical part of the review most of the emphasis will be given to approach (iii) to induce FM bonds since a large number of experimental results can be reproduced by this procedure, but it is important to keep in mind the historical path followed in the understanding of manganites.

Based on all this discussion, it is clear that reasonable proposals to understand the stabilization of AF and FM phases in manganites have been around since the early theoretical studies of manganese oxides. However, these approaches (double exchange, ferromagnetic covalent bonds, and large Hund coupling) are still *not* sufficient to handle the very complex phase diagram of manganites. For instance, there are compounds such as $\text{La}_{1-x}\text{Sr}_x\text{MnO}_3$ that actually do not have the CE-phase at $x=0.5$, while others do. There are compounds that are never metallic, while others have a paramagnetic state with standard metallic characteristics. And even more important, in the early studies of manganites there was no proper rationalization for the large MR effect. It is only with the use of state-of-the-art many-body tools that the large magnetotransport effects are starting to be understood, thanks to theoretical developments in recent years that can address the competition among the different phases of manganites, their clustering and mixed-phase tendencies, and dynamical Jahn-Teller polaron formation.

The prevailing ideas to explain the curious magnetotransport behavior of manganites changed in the mid-90's from the simple double-exchange scenario to a more elaborated picture where a large Jahn-Teller (JT)

effect, which occurs in the Mn^{3+} ions, produces a strong electron-phonon coupling that persists even at densities where a ferromagnetic ground-state is observed. In fact, in the undoped limit $x=0$, and even at finite but small x , it is well-known that a robust static structural distortion is present in the manganites. In this context, it is natural to imagine the existence of small lattice polarons in the paramagnetic phase above T_C , and it was believed that these polarons lead to the insulating behavior of this regime. Actually, the term polaron is somewhat ambiguous. In the context of manganites it is usually associated with a local distortion of the lattice around the charge, sometimes together with a magnetic cloud or region with ferromagnetic correlations (magneto polaron or lattice-magneto polaron).

The fact that double-exchange cannot be enough to understand the physics of manganites is clear from several different points of view. For instance, Millis, Littlewood and Shraiman (1995) arrived at this conclusion by presenting estimations of the critical Curie temperature and of the resistivity using the DE framework. It is clear that the one-orbital model is incomplete for quantitative studies since it cannot describe, e.g., the key orbital-ordering of manganites and the proper charge-order states at x near 0.5, which are so important for the truly CMR effect found in low-bandwidth manganites. Not even a fully disordered set of classical spins can scatter electrons as much as needed to reproduce the experiments (again, unless large antiferromagnetic regions appear in a mixed-phase regime).

Millis, Shraiman and Mueller (1996) (see also Millis, Mueller, and Shraiman, 1996, and Millis, 1998) argued that the physics of manganites is dominated by the interplay between a strong electron-phonon coupling and the large Hund coupling effect that optimizes the electronic kinetic energy by the generation of a FM phase. The large value of the electron phonon coupling is clear in the regime of manganites below $x=0.20$ where a static JT distortion plays a key role in the physics of the material. Millis, Shraiman and Mueller (1996) argued that a dynamical JT effect may persist at higher hole densities, without leading to long-range order but producing important fluctuations that localize electrons by splitting the degenerate e_g levels at a given MnO_6 octahedron. The calculations were carried out using the infinite dimensional approximation that corresponds to a *local* mean-field technique where the polarons can have only a one site extension, and the classical limit for the phonons and spins was used. The Coulomb interactions were neglected, but further work reviewed below showed that JT and Coulombic interactions lead to very similar results (Hotta, Malvezzi, and Dagotto, 2000). Millis, Shraiman and Mueller (1996) argued that the ratio $\lambda_{\text{eff}}=E_{\text{JT}}/t_{\text{eff}}$ domi-

nates the physics of the problem. Here E_{JT} is the static trapping energy at a given octahedron, and t_{eff} is an effective hopping that is temperature dependent following the standard DE discussion. In this context it was conjectured that when the temperature is larger than T_C the effective coupling λ_{eff} could be above the critical value that leads to insulating behavior due to electron localization, while it becomes smaller than the critical value below T_C , thus inducing metallic behavior. However, in order to describe the percolative nature of the transition found experimentally and the notorious phase separation tendencies, calculations beyond mean-field approximations are needed, as reviewed later in this paper. Similar phase separation ideas have been discussed extensively in the context of high temperature superconductors as well (see Emery, Kivelson, and Lin, 1990. See also Tranquada et al., 1995).

2. Model for Manganites

Before proceeding to a description of the latest theoretical developments, it is necessary to clearly write down the model Hamiltonian for manganites. For complex materials such as the Mn-oxides, unfortunately, the full Hamiltonian includes several competing tendencies and couplings. However, as shown below, the essential physics can be obtained using relatively simple models, deduced from the complicated full Hamiltonian.

2.1 Crystal field effect

In order to construct the model Hamiltonian for manganites, let us start our discussion at the level of the atomic problem, in which just one electron occupies a certain orbital in the $3d$ shell of a manganese ion. Although for an isolated ion a five-fold degeneracy exists for the occupation of the $3d$ orbitals, this degeneracy is partially lifted by the crystal field due to the six oxygen ions surrounding the manganese forming an octahedron. This is analyzed by the ligand field theory that shows that the five-fold degeneracy is lifted into doubly-degenerate e_g -orbitals ($d_{x^2-y^2}$ and $d_{3z^2-r^2}$) and triply-degenerate t_{2g} -orbitals (d_{xy} , d_{yz} , and d_{zx}). The energy difference between those two levels is usually expressed as $10Dq$, by following the traditional notation in the ligand field theory.

Here note that the energy level for the t_{2g} -orbitals is lower than that for e_g -orbitals. Qualitatively this can be understood as follows: The energy difference originates in the Coulomb interaction between the $3d$ electrons and the oxygen ions surrounding manganese. While the wavefunctions of the e_g -orbitals is extended along the direction of the bond between manganese and oxygen ions, those in the t_{2g} -orbitals avoid this

direction. Thus, an electron in t_{2g} -orbitals is not heavily influenced by the Coulomb repulsion due to the negatively charged oxygen ions, and the energy level for t_{2g} -orbitals is lower than that for e_g -orbitals.

As for the value of $10Dq$, it is explicitly written as (see Gerloch and Slade, 1973)

$$10Dq = \frac{5}{3} \frac{Ze^2}{a} \frac{\langle r^4 \rangle}{a^4}, \quad (1.1)$$

where Z is the atomic number of the ligand ion, e is the electron charge, a is the distance between manganese and oxygen ions, r is the coordinate of the $3d$ orbital, and $\langle \dots \rangle$ denotes the average value by using the radial wavefunction of the $3d$ orbital. Estimations by Yoshida (page 29 of Yoshida, 1996) suggest that $10Dq$ is about $10000\text{--}15000\text{cm}^{-1}$ (remember that $1\text{eV} = 8063\text{ cm}^{-1}$).

2.2 Coulomb interactions

Now consider a Mn^{4+} ion, in which three electrons exist in the $3d$ shells. Although those electrons will occupy t_{2g} -orbitals due to the crystalline field splitting, the configuration is not uniquely determined. To configure three electrons appropriately, it is necessary to take into account the effect of the Coulomb interactions. In the localized ion system, the Coulomb interaction term among d -electrons is generally given by

$$H_{\mathbf{i}}^{\text{C}} = \frac{1}{2} \sum_{\gamma_1 \gamma_2 \gamma'_1 \gamma'_2} \sum_{\sigma_1 \sigma_2 \sigma'_1 \sigma'_2} I_{\gamma_1 \sigma_1, \gamma_2 \sigma_2; \gamma'_1 \sigma'_1, \gamma'_2 \sigma'_2} d_{\mathbf{i} \gamma_1 \sigma_1}^\dagger d_{\mathbf{i} \gamma_2 \sigma_2}^\dagger d_{\mathbf{i} \gamma'_2 \sigma'_2} d_{\mathbf{i} \gamma'_1 \sigma'_1}, \quad (1.2)$$

where $d_{\mathbf{i} \gamma \sigma}$ is the annihilation operator for a d -electron with spin σ in the γ -orbital at site \mathbf{i} , and the Coulomb matrix element is given by

$$I_{\gamma_1 \sigma_1, \gamma_2 \sigma_2; \gamma'_1 \sigma'_1, \gamma'_2 \sigma'_2} = \int \int d\mathbf{r} d\mathbf{r}' \phi_{\gamma_1 \sigma_1}^*(\mathbf{r}) \phi_{\gamma_2 \sigma_2}^*(\mathbf{r}') g_{\mathbf{r}-\mathbf{r}'} \phi_{\gamma'_1 \sigma'_1}(\mathbf{r}) \phi_{\gamma'_2 \sigma'_2}(\mathbf{r}'). \quad (1.3)$$

Here $g_{\mathbf{r}-\mathbf{r}'}$ is the screened Coulomb potential, and $\phi_{\gamma \sigma}(\mathbf{r})$ is the Wannier function for an electron with spin σ in the γ -orbital at position \mathbf{r} . By using the Coulomb matrix element, the so-called ‘‘Kanamori parameters’’, U , U' , J , and J' , are defined as follows (see Kanamori, 1963; Dworin and Narath, 1970; Castellani et al., 1978). U is the intraband Coulomb interaction, given by

$$U = I_{\gamma \sigma, \gamma \sigma; \gamma \sigma, \gamma \sigma}, \quad (1.4)$$

with $\sigma \neq \sigma'$. U' is the interband Coulomb interaction, expressed by

$$U' = I_{\gamma \sigma, \gamma' \sigma'; \gamma \sigma, \gamma' \sigma'}, \quad (1.5)$$

with $\gamma \neq \gamma'$. J is the interband exchange interaction, written as

$$J = I_{\gamma\sigma,\gamma'\sigma';\gamma'\sigma,\gamma\sigma'}, \quad (1.6)$$

with $\gamma \neq \gamma'$. Finally, J' is the pair-hopping amplitude between different orbitals, given by

$$J' = I_{\gamma\sigma,\gamma\sigma';\gamma'\sigma,\gamma'\sigma'}, \quad (1.7)$$

with $\gamma \neq \gamma'$ and $\sigma \neq \sigma'$.

Note the relation $J=J'$, which is simply due to the fact that each of the parameters above is given by an integral of the Coulomb interaction sandwiched with appropriate orbital wave functions. Analyzing the form of those integrals the equality between J and J' can be deduced [see Eq. (2.6) of Castellani et al., 1978; See also the Appendix of Frésard and Kotliar, 1997]. Using the above parameters, it is convenient to rewrite the Coulomb interaction term in the following form:

$$\begin{aligned} H_{\mathbf{i}}^{\text{C}} &= \frac{U}{2} \sum_{\gamma,\sigma \neq \sigma'} n_{\mathbf{i}\gamma\sigma} n_{\mathbf{i}\gamma\sigma'} + \frac{U'}{2} \sum_{\sigma,\sigma',\gamma \neq \gamma'} n_{\mathbf{i}\gamma\sigma} n_{\mathbf{i}\gamma'\sigma'} \\ &+ \frac{J}{2} \sum_{\sigma,\sigma',\gamma \neq \gamma'} d_{\mathbf{i}\gamma\sigma}^{\dagger} d_{\mathbf{i}\gamma'\sigma'}^{\dagger} d_{\mathbf{i}\gamma\sigma'} d_{\mathbf{i}\gamma'\sigma} \\ &+ \frac{J'}{2} \sum_{\sigma \neq \sigma',\gamma \neq \gamma'} d_{\mathbf{i}\gamma\sigma}^{\dagger} d_{\mathbf{i}\gamma\sigma'}^{\dagger} d_{\mathbf{i}\gamma'\sigma'} d_{\mathbf{i}\gamma'\sigma}, \end{aligned} \quad (1.8)$$

where $n_{\mathbf{i}\gamma\sigma} = d_{\mathbf{i}\gamma\sigma}^{\dagger} d_{\mathbf{i}\gamma\sigma}$. Here it is important to clarify that the parameters U , U' , and J are not independent (here $J=J'$ is used). The relation among them in the localized ion problem has been clarified by group theory arguments, showing that all the above Coulomb interactions can be expressed by the so-called ‘‘Racah parameters’’ (for more details, see Griffith, 1961. See also Tang, Plihal, and Mills, 1998). By using those expressions for U , U' and J , it is easily checked that the relation

$$U = U' + 2J \quad (1.9)$$

holds in any combination of orbitals. Note that this relation is needed to recover the rotational invariance in orbital space. For more details the reader should consult Dagotto, Hotta, and Moreo, 2001.

Now let us move to the discussion of the configuration of three electrons for the Mn^{4+} ion. Since the largest energy scale among the several Coulombic interactions is U , the orbitals are not doubly occupied by both up- and down-spin electrons. Thus, only one electron can exist in

each orbital of the triply degenerate t_{2g} sector. Furthermore, in order to take advantage of J , the spins of those three electrons point along the same direction. This is the so-called ‘‘Hund’s rule’’.

By adding one more electron to Mn^{4+} with three up-spin t_{2g} -electrons, let us consider the configuration for the Mn^{3+} ion. Note here that there are two possibilities due to the balance between the crystalline-field splitting and the Hund coupling: One is the ‘‘high-spin state’’ in which an electron occupies the e_g -orbital with up spin if the Hund coupling is dominant. In this case, the energy level appears at $U' - J + 10Dq$. Another is the ‘‘low-spin state’’ in which one of the t_{2g} -orbitals is occupied with a down-spin electron, when the crystalline-field splitting is much larger than the Hund coupling. In this case, the energy level occurs at $U + 2J$. Thus, the high spin state appears if $10Dq < 5J$ holds. Since J is a few eV and $10Dq$ is about 1eV in the manganese oxide, the inequality $10Dq < 5J$ is considered to hold. Namely, in the Mn^{3+} ion, the high spin state is realized.

In order to simplify the model without loss of essential physics, it is reasonable to treat the three spin-polarized t_{2g} -electrons as a localized ‘‘core-spin’’ expressed by \mathbf{S}_i at site i , since the overlap integral between t_{2g} and oxygen $p\sigma$ orbital is small compared to that between e_g and $p\sigma$ orbitals. Moreover, due to the large value of the total spin $S=3/2$, it is usually approximated by a classical spin (this approximation will be tested later using computational techniques). Thus, the effect of the strong Hund coupling between the e_g -electron spin and localized t_{2g} -spins is considered by introducing

$$H_{\text{Hund}} = -J_H \sum_i \mathbf{s}_i \cdot \mathbf{S}_i, \quad (1.10)$$

where $\mathbf{s}_i = \sum_{\gamma\alpha\beta} d_{i\gamma\alpha}^\dagger \sigma_{\alpha\beta} d_{i\gamma\beta}$, $J_H(>0)$ is the Hund coupling between localized t_{2g} -spin and mobile e_g -electron, and $\sigma=(\sigma_x, \sigma_y, \sigma_z)$ are the Pauli matrices. The magnitude of J_H is of the order of J . Here note that \mathbf{S}_i is normalized as $|\mathbf{S}_i|=1$. Thus, the direction of the classical t_{2g} -spin at site i is defined as

$$\mathbf{S}_i = (\sin \theta_i \cos \phi_i, \sin \theta_i \sin \phi_i, \cos \theta_i), \quad (1.11)$$

by using the polar angle θ_i and the azimuthal angle ϕ_i .

Unfortunately, the effect of the Coulomb interaction is not fully taken into account only by H_{Hund} since there remains the direct electrostatic repulsion between e_g -electrons, which will be referred to as the ‘‘Coulomb interaction’’ hereafter. Then, the following term should be added to the

Hamiltonian.

$$H_{\text{el-el}} = \sum_{\mathbf{i}} H_{\mathbf{i}}^{\text{C}} + V \sum_{\langle \mathbf{i}, \mathbf{j} \rangle} \rho_{\mathbf{i}} \rho_{\mathbf{j}}, \quad (1.12)$$

where $\rho_{\mathbf{i}} = \sum_{\gamma\sigma} n_{\mathbf{i}\gamma\sigma}$. Note here that in this expression, the index γ for the orbital degree of freedom runs only in the e_g -sector. Note also that in order to consider the effect of the long-range Coulomb repulsion between e_g -electrons, the term including V is added, where V is the nearest-neighbor Coulomb interaction.

2.3 Electron-phonon coupling

Another important ingredient in manganites is the lattice distortion coupled to the e_g -electrons. In particular, the double degeneracy in the e_g -orbitals is lifted by the Jahn-Teller distortion of the MnO_6 octahedron (Jahn and Teller, 1937). The basic formalism for the study of electrons coupled to Jahn-Teller modes has been set up by Kanamori, 1960. He focused on cases where the electronic orbitals are degenerate in the undistorted crystal structure, as in the case of Mn in an octahedron of oxygens. As explained by Kanamori, the Jahn-Teller effect in this context can be simply stated as follows; when a given electronic level of a cluster is degenerate in a structure of high symmetry, this structure is generally unstable, and the cluster will present a distortion toward a lower symmetry ionic arrangement. In the case of Mn^{3+} , which is doubly degenerate when the crystal is undistorted, a splitting will occur when the crystal is distorted. The distortion of the MnO_6 octahedron is “cooperative” since once it occurs in a particular octahedron, it will affect the neighbors. The basic Hamiltonian to describe the interaction between electrons and Jahn-Teller modes was written by Kanamori and it is of the form

$$H_{\mathbf{i}}^{\text{JT}} = g(Q_{2\mathbf{i}}T_{\mathbf{i}}^x + Q_{3\mathbf{i}}T_{\mathbf{i}}^z) + (k_{\text{JT}}/2)(Q_{2\mathbf{i}}^2 + Q_{3\mathbf{i}}^2), \quad (1.13)$$

where g is the coupling constant between the e_g -electrons and distortions of the MnO_6 octahedron, $Q_{2\mathbf{i}}$ and $Q_{3\mathbf{i}}$ are normal modes of vibration of the oxygen octahedron that remove the degeneracy between the electronic levels, and k_{JT} is the spring constant for the Jahn-Teller mode distortions. The pseudospin operators are defined as

$$T_{\mathbf{i}}^x = \sum_{\sigma} (d_{\mathbf{i}a\sigma}^{\dagger} d_{\mathbf{i}b\sigma} + d_{\mathbf{i}b\sigma}^{\dagger} d_{\mathbf{i}a\sigma}), \quad T_{\mathbf{i}}^z = \sum_{\sigma} (d_{\mathbf{i}a\sigma}^{\dagger} d_{\mathbf{i}a\sigma} - d_{\mathbf{i}b\sigma}^{\dagger} d_{\mathbf{i}b\sigma}). \quad (1.14)$$

In the expression of $H_{\mathbf{i}}^{\text{JT}}$, a $T_{\mathbf{i}}^y$ -term does not appear for symmetry reasons, since it belongs to the A_{2u} representation. The non-zero terms should correspond to the irreducible representations included in $E_g \times E_g$,

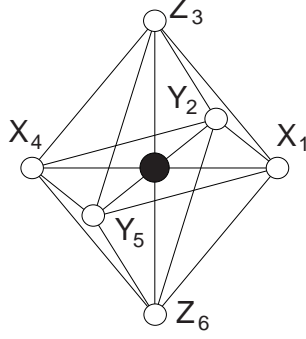


Figure 1.1. MnO_6 octahedron at site \mathbf{i} . The labeling for oxygen ions is shown.

namely, E_g and A_{1g} . The former representation is expressed by using the pseudo spin operators $T_{\mathbf{i}}^x$ and $T_{\mathbf{i}}^z$ as discussed here, while the latter, corresponding to the breathing mode, is discussed later.

Following Kanamori, $Q_{2\mathbf{i}}$ and $Q_{3\mathbf{i}}$ are explicitly given by

$$Q_{2\mathbf{i}} = \frac{1}{\sqrt{2}}(X_{1\mathbf{i}} - X_{4\mathbf{i}} - Y_{2\mathbf{i}} + Y_{5\mathbf{i}}), \quad (1.15)$$

and

$$Q_{3\mathbf{i}} = \frac{1}{\sqrt{6}}(2Z_{3\mathbf{i}} - 2Z_{6\mathbf{i}} - X_{1\mathbf{i}} + X_{4\mathbf{i}} - Y_{2\mathbf{i}} + Y_{5\mathbf{i}}), \quad (1.16)$$

where $X_{\mu j}$, $Y_{\mu j}$, and $Z_{\mu j}$ are the displacement of oxygen ions from the equilibrium positions along the x -, y -, and z -direction, respectively. The convention for the labeling μ of coordinates is shown in Fig. 1.1.

To solve this Hamiltonian, it is convenient to scale the phononic degrees of freedom as

$$Q_{2\mathbf{i}} = (g/k_{\text{JT}})q_{2\mathbf{i}}, \quad Q_{3\mathbf{i}} = (g/k_{\text{JT}})q_{3\mathbf{i}}, \quad (1.17)$$

where g/k_{JT} is the typical length scale for the Jahn-Teller distortion, which is of the order of 0.1\AA , namely, 2.5% of the lattice constant. When the Jahn-Teller distortion is expressed in the polar coordinate as

$$q_{2\mathbf{i}} = q_{\mathbf{i}} \sin \xi_{\mathbf{i}}, \quad q_{3\mathbf{i}} = q_{\mathbf{i}} \cos \xi_{\mathbf{i}}, \quad (1.18)$$

the ground state is easily obtained as $(-\sin[\xi_{\mathbf{i}}/2]d_{\mathbf{i}a\sigma}^\dagger + \cos[\xi_{\mathbf{i}}/2]d_{\mathbf{i}b\sigma}^\dagger)|0\rangle$ with the use of the phase $\xi_{\mathbf{i}}$. The corresponding eigenenergy is given by $-E_{\text{JT}}$, where E_{JT} is the static Jahn-Teller energy, defined by

$$E_{\text{JT}} = g^2/(2k_{\text{JT}}). \quad (1.19)$$

Note here that the ground state energy is independent of the phase ξ_i . Namely, the shape of the deformed isolated octahedron is not uniquely determined in this discussion. In the Jahn-Teller crystal, the kinetic motion of e_g electrons, as well as the cooperative effect between adjacent distortions, play a crucial role in lifting the degeneracy and fixing the shape of the local distortion.

To complete the electron-phonon coupling term, it is necessary to consider the breathing mode distortion, coupled to the local electron density as

$$H_i^{\text{br}} = gQ_{1i}\rho_i + (1/2)k_{\text{br}}Q_{1i}^2, \quad (1.20)$$

where the breathing-mode distortion Q_{1i} is given by

$$Q_{1i} = \frac{1}{\sqrt{3}}(X_{1i} - X_{4i} + Y_{2i} - Y_{5i} + Z_{3i} - Z_{6i}), \quad (1.21)$$

and k_{br} is the associated spring constant. Note that, in principle, the coupling constants of the e_g electrons with the Q_1 , Q_2 , and Q_3 modes could be different from one another. For simplicity, here it is assumed that those coupling constants take the same value. On the other hand, for the spring constants, a different notation for the breathing mode is introduced, since the frequency for the breathing mode distortion has been found experimentally to be different from that for the Jahn-Teller mode. This point will be briefly discussed later. Note also that the Jahn-Teller and breathing modes are competing with each other. As it was shown above, the energy gain due to the Jahn-Teller distortion is maximized when one electron exists per site. On the other hand, the breathing mode distortion energy is proportional to the total number of e_g electrons per site, since this distortion gives rise to an effective on-site attraction between electrons.

By combining the Jahn-Teller mode and breathing mode distortions, the electron-phonon term is summarized as

$$H_{\text{el-ph}} = \sum_i (H_i^{\text{JT}} + H_i^{\text{br}}). \quad (1.22)$$

This expression depends on the parameter $\beta = k_{\text{br}}/k_{\text{JT}}$, which regulates which distortion, the Jahn-Teller or breathing mode, play a more important role. This point will be discussed in a separate subsection.

Note again that the distortions at each site are not independent, since all oxygens are shared by neighboring MnO_6 octahedra, as easily understood by the explicit expressions of Q_{1i} , Q_{2i} , and Q_{3i} presented before. A direct and simple way to consider this cooperative effect is to determine the oxygen positions X_{1i} , X_{4i} , Y_{2i} , Y_{5i} , Z_{3i} , and Z_{6i} , by using, for

instance, the Monte Carlo simulations or numerical relaxation methods (see Press et al., 1992, chapter 10). To reduce the burden on the numerical calculations, the displacements of oxygen ions are assumed to be along the bond direction between nearest neighboring manganese ions. In other words, the displacement of the oxygen ion perpendicular to the Mn-Mn bond, i.e., the buckling mode, is usually ignored. As shown later, even in this simplified treatment, several interesting results have been obtained for the spin, charge, and orbital ordering in manganites.

Rewriting Eqs. (1.15), (1.16), and (1.21) in terms of the displacement of oxygens from the equilibrium positions, it can be shown that

$$Q_{1i} = Q_1^{(0)} + \frac{1}{\sqrt{3}}(\Delta_{xi} + \Delta_{yi} + \Delta_{zi}), \quad (1.23)$$

$$Q_{2i} = Q_2^{(0)} + \frac{1}{\sqrt{2}}(\Delta_{xi} - \Delta_{yi}), \quad (1.24)$$

$$Q_{3i} = Q_3^{(0)} + \frac{1}{\sqrt{6}}(2\Delta_{zi} - \Delta_{xi} - \Delta_{yi}), \quad (1.25)$$

where Δ_{ai} is given by

$$\Delta_{ai} = u_i^a - u_{i-a}^a, \quad (1.26)$$

with u_i^a being the displacement of oxygen ion at site i from the equilibrium position along the a -axis. The offset values for the distortions, $Q_1^{(0)}$, $Q_2^{(0)}$, and $Q_3^{(0)}$, are respectively given by

$$Q_1^{(0)} = \frac{1}{\sqrt{3}}(\delta L_x + \delta L_y + \delta L_z), \quad (1.27)$$

$$Q_2^{(0)} = \frac{1}{\sqrt{2}}(\delta L_x - \delta L_y), \quad (1.28)$$

$$Q_3^{(0)} = \frac{1}{\sqrt{6}}(2\delta L_z - \delta L_x - \delta L_y), \quad (1.29)$$

where $\delta L_a = L_a - L$, the non-distorted lattice constants are L_a , and $L = (L_x + L_y + L_z)/3$. In the *cooperative* treatment, the $\{u\}$'s are directly optimized in the numerical calculations (see Allen and Perebeinos, 1999; Hotta et al. 1999). On the other hand, in the *non-cooperative* calculations, $\{Q\}$'s are treated instead of the $\{u\}$'s. In the simulations, variables are taken as $\{Q\}$'s or $\{u\}$'s, depending on the treatments of lattice distortion.

2.4 Hopping amplitudes

Although it is assumed that the t_{2g} -electrons are localized to form core spins, the e_g -electrons can move around the system via the oxygen $2p$ orbital. This hopping motion of e_g -electrons is expressed as

$$H_{\text{kin}} = - \sum_{\mathbf{ia}\gamma\gamma'\sigma} t_{\gamma\gamma'}^{\mathbf{a}} d_{\mathbf{i}\gamma\sigma}^\dagger d_{\mathbf{i}+\mathbf{a}\gamma'\sigma}, \quad (1.30)$$

where \mathbf{a} is the vector connecting nearest-neighbor sites and $t_{\gamma\gamma'}^{\mathbf{a}}$ is the nearest-neighbor hopping amplitude between γ - and γ' -orbitals along the \mathbf{a} -direction.

The amplitudes are evaluated from the overlap integral between manganese and oxygen ions by following Slater and Koster (1954). The overlap integral between $d_{x^2-y^2}$ - and p_x -orbitals is given by

$$E_{\mathbf{x},\mathbf{a}}(\ell, m, n) = (\sqrt{3}/2)\ell(\ell^2 - m^2)(pd\sigma), \quad (1.31)$$

where $(pd\sigma)$ is the overlap integral between the $d\sigma$ - and $p\sigma$ -orbital and (ℓ, m, n) is the unit vector along the direction from manganese to oxygen ions. The overlap integral between $d_{3z^2-r^2}$ - and p_x -orbitals is expressed as

$$E_{\mathbf{x},\mathbf{b}}(\ell, m, n) = \ell[n^2 - (\ell^2 + m^2)/2](pd\sigma). \quad (1.32)$$

Thus, the hopping amplitude between adjacent manganese ions along the x -axis via the oxygen $2p_x$ -orbitals is evaluated as

$$-t_{\gamma\gamma'}^{\mathbf{x}} = E_{\mathbf{x},\gamma}(1, 0, 0) \times E_{\mathbf{x},\gamma'}(-1, 0, 0). \quad (1.33)$$

Note here that the minus sign is due to the definition of hopping amplitude in H_{kin} . Then, $t_{\gamma\gamma'}^{\mathbf{x}}$ is explicitly given by

$$t_{\text{aa}}^{\mathbf{x}} = -\sqrt{3}t_{\text{ab}}^{\mathbf{x}} = -\sqrt{3}t_{\text{ba}}^{\mathbf{x}} = 3t_{\text{bb}}^{\mathbf{x}} = 3t_0/4, \quad (1.34)$$

where t_0 is defined by $t_0 = (pd\sigma)^2/|\varepsilon_d - \varepsilon_p|$. Here ε_d and ε_p are the energy level for d - and p -orbitals. By using the same procedure, the hopping amplitude along the y - and z -axis are given by

$$t_{\text{aa}}^{\mathbf{y}} = \sqrt{3}t_{\text{ab}}^{\mathbf{y}} = \sqrt{3}t_{\text{ba}}^{\mathbf{y}} = 3t_{\text{bb}}^{\mathbf{y}} = 3t_0/4, \quad (1.35)$$

and

$$t_{\text{bb}}^{\mathbf{z}} = t_0, t_{\text{aa}}^{\mathbf{z}} = t_{\text{ab}}^{\mathbf{z}} = t_{\text{ba}}^{\mathbf{z}} = 0, \quad (1.36)$$

respectively. It should be noted that the signs in the hopping amplitudes between different orbitals are different between the x - and y -directions, which will be important when the charge-orbital ordered phase in the doped manganites is considered. Note also that in some cases, it is convenient to define $t_{\text{aa}}^{\mathbf{x}}$ as the energy scale t , given as $t=3t_0/4$.

2.5 Heisenberg term

Thus far, the role of the e_g -electrons has been discussed to characterize the manganites. However, in the fully hole-doped manganites composed of Mn^{4+} ions, for instance CaMnO_3 , it is well known that a G-type antiferromagnetic phase appears, and this property cannot be understood within the above discussion. The minimal term to reproduce this antiferromagnetic property is the Heisenberg-like coupling between localized t_{2g} spins, given in the form

$$H_{\text{AFM}} = J_{\text{AF}} \sum_{\langle \mathbf{i}, \mathbf{j} \rangle} \mathbf{S}_{\mathbf{i}} \cdot \mathbf{S}_{\mathbf{j}}, \quad (1.37)$$

where J_{AF} is the AFM coupling between nearest neighbor t_{2g} spins. The existence of this term is quite natural from the viewpoint of the super-exchange interaction, working between neighboring localized t_{2g} -electrons. As for the magnitude of J_{AF} , it is discussed later in the text.

2.6 Several Hamiltonians

As discussed in the previous subsections, there are five important ingredients that regulate the physics of electrons in manganites: (i) H_{kin} , the kinetic term of the e_g electrons. (ii) H_{Hund} , the Hund coupling between the e_g electron spin and the localized t_{2g} spin. (iii) H_{AFM} , the AFM Heisenberg coupling between nearest neighbor t_{2g} spins. (iv) $H_{\text{el-ph}}$, the coupling between the e_g electrons and the local distortions of the MnO_6 octahedron. (v) $H_{\text{el-el}}$, the Coulomb interactions among the e_g electrons. As schematically summarized in Fig. 1.2, by unifying those five terms into one, the full Hamiltonian H is defined as

$$H = H_{\text{kin}} + H_{\text{Hund}} + H_{\text{AFM}} + H_{\text{el-ph}} + H_{\text{el-el}}. \quad (1.38)$$

This expression is believed to define an appropriate starting model for manganites, but unfortunately, it is quite difficult to solve such a Hamiltonian. In order to investigate further the properties of manganites, some simplifications are needed. In below, several types of simplified models are listed.

2.6.1 One-orbital Model

A simple model for manganites to illustrate the CMR effect is obtained by neglecting the electron-phonon coupling and the Coulomb interactions. Usually, an extra simplification is carried out by neglecting the orbital degrees of freedom, leading to the FM Kondo model or one-orbital double-exchange model, which will be simply referred as the

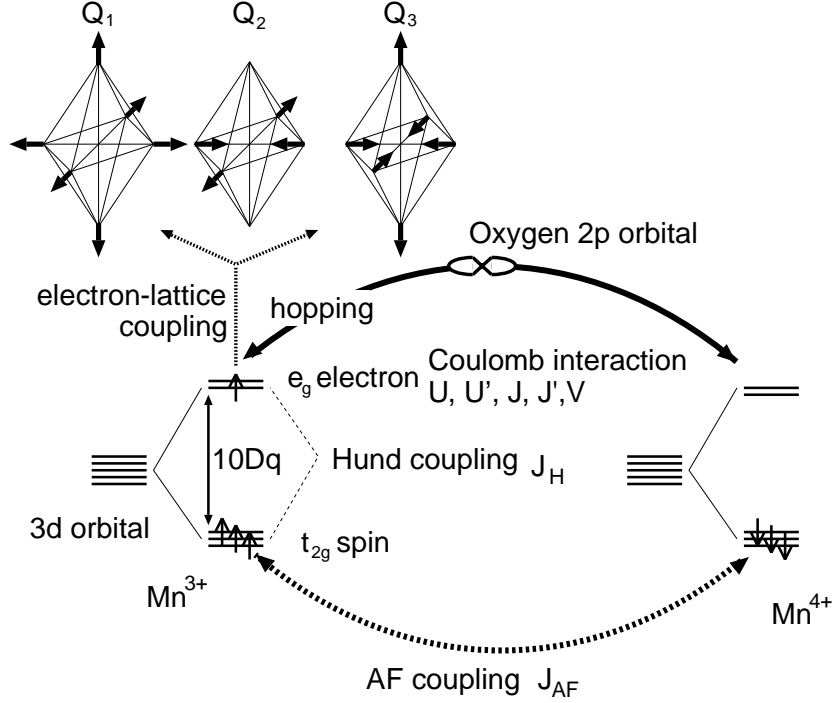


Figure 1.2. Schematic figure of the model Hamiltonian for manganites.

“one-orbital model” hereafter, given as (Zener, 1951; Furukawa, 1994)

$$H_{\text{DE}} = -t \sum_{\langle \mathbf{i}, \mathbf{j} \rangle, \sigma} (a_{\mathbf{i}\sigma}^\dagger a_{\mathbf{j}\sigma} + \text{H.c.}) - J_{\text{H}} \sum_{\mathbf{i}} \mathbf{s}_{\mathbf{i}} \cdot \mathbf{S}_{\mathbf{j}} + J_{\text{AF}} \sum_{\langle \mathbf{i}, \mathbf{j} \rangle} \mathbf{S}_{\mathbf{i}} \cdot \mathbf{S}_{\mathbf{j}}, \quad (1.39)$$

where $a_{\mathbf{i}\sigma}$ is the annihilation operator for an electron with spin σ at site \mathbf{i} , but without orbital index. Note that H_{DE} is quadratic in the electron operators, indicating that it is reduced to a one-electron problem on the background of localized t_{2g} spins. This is a clear advantage for the Monte Carlo simulations. Neglecting the orbital degrees of freedom is clearly an oversimplification, and important phenomena such as orbital ordering cannot be obtained in this model. However, the one-orbital model is still important, since it already includes part of the essence of manganese oxides. For example, recent computational investigations have clarified that the very important phase separation tendencies and metal-insulator competition exist in this model.

2.6.2 $J_H = \infty$ limit

Another simplification without the loss of essential physics is to take the widely used limit $J_H = \infty$, since in the actual material J_H/t is much larger than unity. In such a limit, the e_g -electron spin perfectly aligns along the t_{2g} -spin direction, reducing the number of degrees of freedom. Then, in order to diagonalize the Hund term, the “spinless” e_g -electron operator, $c_{\mathbf{i}\gamma}$, is defined as

$$c_{\mathbf{i}\gamma} = \cos(\theta_{\mathbf{i}}/2)d_{\mathbf{i}\gamma\uparrow} + \sin(\theta_{\mathbf{i}}/2)e^{-i\phi_{\mathbf{i}}}d_{\mathbf{i}\gamma\downarrow}. \quad (1.40)$$

In terms of the c -variables, the kinetic energy acquires the simpler form

$$H_{\text{kin}} = - \sum_{\mathbf{i}\mathbf{a}\gamma\gamma'} \tilde{t}_{\gamma\gamma'}^{\mathbf{a}} c_{\mathbf{i}\gamma}^{\dagger} c_{\mathbf{i}+\mathbf{a}\gamma'}, \quad (1.41)$$

where $\tilde{t}_{\gamma\gamma'}^{\mathbf{a}}$ is defined as $\tilde{t}_{\gamma\gamma'}^{\mathbf{a}} = S_{\mathbf{i},\mathbf{i}+\mathbf{a}} t_{\gamma\gamma'}^{\mathbf{a}}$ with $S_{\mathbf{i},\mathbf{j}}$ given by

$$S_{\mathbf{i},\mathbf{j}} = \cos(\theta_{\mathbf{i}}/2) \cos(\theta_{\mathbf{j}}/2) + \sin(\theta_{\mathbf{i}}/2) \sin(\theta_{\mathbf{j}}/2) e^{-i(\phi_{\mathbf{i}} - \phi_{\mathbf{j}})}. \quad (1.42)$$

This factor denotes the change of hopping amplitude due to the difference in angles between t_{2g} -spins at sites \mathbf{i} and \mathbf{j} . Note that the effective hopping in this case is a complex number (Berry phase), contrary to the real number widely used in a large number of previous investigations (for details in the case of the one-orbital model see Müller-Hartmann and Dagotto, 1996).

The limit of infinite Hund coupling reduces the number of degrees of freedom substantially since the spin index is no longer needed. In addition, the U - and J -terms in the electron-electron interaction within the e_g -sector are also no longer needed. In this case, the following simplified model is obtained:

$$\begin{aligned} H^{\infty} = & - \sum_{\mathbf{i}\mathbf{a}\gamma\gamma'} \tilde{t}_{\gamma\gamma'}^{\mathbf{a}} c_{\mathbf{i}\gamma}^{\dagger} c_{\mathbf{i}+\mathbf{a}\gamma'} + U' \sum_{\mathbf{i}} n_{\mathbf{i}\mathbf{a}} n_{\mathbf{i}\mathbf{b}} + V \sum_{\langle \mathbf{i}, \mathbf{j} \rangle} n_{\mathbf{i}} n_{\mathbf{j}} + J_{\text{AF}} \sum_{\langle \mathbf{i}, \mathbf{j} \rangle} \mathbf{S}_{\mathbf{i}} \cdot \mathbf{S}_{\mathbf{j}} \\ & + E_{\text{JT}} \sum_{\mathbf{i}} [2(q_{1\mathbf{i}} n_{\mathbf{i}} + q_{2\mathbf{i}} \tau_{xi} + q_{3\mathbf{i}} \tau_{zi}) + \beta q_{1\mathbf{i}}^2 + q_{2\mathbf{i}}^2 + q_{3\mathbf{i}}^2], \end{aligned} \quad (1.43)$$

where $n_{\mathbf{i}\gamma} = c_{\mathbf{i}\gamma}^{\dagger} c_{\mathbf{i}\gamma}$, $n_{\mathbf{i}} = \sum_{\gamma} n_{\mathbf{i}\gamma}$, $\tau_{xi} = c_{\mathbf{i}\mathbf{a}}^{\dagger} c_{\mathbf{i}\mathbf{b}} + c_{\mathbf{i}\mathbf{b}}^{\dagger} c_{\mathbf{i}\mathbf{a}}$, and $\tau_{zi} = c_{\mathbf{i}\mathbf{a}}^{\dagger} c_{\mathbf{i}\mathbf{a}} - c_{\mathbf{i}\mathbf{b}}^{\dagger} c_{\mathbf{i}\mathbf{b}}$.

Considering the simplified Hamiltonian H^{∞} , two other limiting models can be obtained. One is the Jahn-Teller model H_{JT}^{∞} , defined as $H_{\text{JT}}^{\infty} = H^{\infty}(U' = V = 0)$, in which the Coulomb interactions are simply ignored. Another is the Coulombic model H_{C}^{∞} , defined as $H_{\text{C}}^{\infty} = H^{\infty}(E_{\text{JT}} = 0)$, which denotes the two-orbital double exchange model influenced by the Coulomb interactions, neglecting the phonons. Of course, the actual

situation is characterized by $U' \neq 0$, $V \neq 0$, and $E_{\text{JT}} \neq 0$, but in the spirit of the adiabatic continuation, it is convenient and quite meaningful to consider the minimal models possible to describe correctly the complicated properties of manganites.

2.6.3 Jahn-Teller phononic and Coulombic models

Another possible simplification could have been obtained by neglecting the electron-electron interaction in the full Hamiltonian but keeping the Hund coupling finite, leading to the following purely Jahn-Teller phononic model with active spin degrees of freedom:

$$H_{\text{JT}} = H_{\text{kin}} + H_{\text{Hund}} + H_{\text{AFM}} + H_{\text{el-ph}}. \quad (1.44)$$

Often in this chapter, this Hamiltonian will be referred to as the “two-orbital” model (unless explicitly stated otherwise). To solve H_{JT} , numerical methods such as Monte Carlo techniques and the relaxation method have been employed. Qualitatively, the negligible values of the probability of double occupancy in the strong electron-phonon coupling region with large J_{H} justifies the neglect of $H_{\text{el-el}}$, since the Jahn-Teller energy is maximized when one e_g electron exists at each site. Thus, the Jahn-Teller phonon induced interaction will produce physics quite similar to that due to the on-site correlation.

It would be important to verify this last expectation by studying a multi-orbital model with only Coulombic terms, without the extra approximation of using mean-field techniques for its analysis. Of particular relevance is whether phase separation tendencies and charge ordering appear in this case, as they do in the Jahn-Teller phononic model. This analysis is particularly important since, as explained before, a mixture of phononic and Coulombic interactions is expected to be needed for a proper quantitative description of manganites. For this purpose, yet another simplified model has been analyzed in the literature:

$$H_{\text{C}} = H_{\text{kin}} + H_{\text{el-el}}. \quad (1.45)$$

Note that the Hund coupling term between e_g electrons and t_{2g} spins is not explicitly included. The reason for this extra simplification is that the numerical complexity in the analysis of the model is drastically reduced by neglecting the localized t_{2g} spins. In the FM phase, this is an excellent approximation, but not necessarily for other magnetic arrangements. Nevertheless the authors believe that it is important to establish with accurate numerical techniques whether the phase separation tendencies are already present in this simplified two-orbital models with Coulomb interactions, even if not all degrees of freedom are incorporated from the outset. Adding the $S=3/2$ quantum localized spins to

the problem would considerably increase the size of the Hilbert space of the model, making it intractable with current computational techniques.

2.7 Estimations of Parameters

In this subsection, estimations of the couplings that appear in the models described before are provided. However, before proceeding with the details the reader must be warned that such estimations are actually quite difficult, for the simple reason that in order to compare experiments with theory reliable calculations must be carried out. Needless to say, strong coupling many-body problems are notoriously difficult and complex, and it is quite hard to find accurate calculations to compare against experiments. Then, the numbers quoted below must be taken simply as rough estimations of orders of magnitude. The reader should consult the cited references to analyze the reliability of the estimations mentioned here. Note also that the references discussed in this subsection correspond to only a small fraction of the vast literature on the subject. Nevertheless, the “sample” cited below is representative of the currently accepted trends in manganites.

Regarding the largest energy scales, the on-site U repulsion was estimated to be 5.2 ± 0.3 eV and 3.5 ± 0.3 eV, for CaMnO_3 and LaMnO_3 , respectively, by Park et al. (1996) using photoemission techniques. The charge-transfer energy has been found to be 3.0 ± 0.5 eV for CaMnO_3 in the same study. In other photoemission studies, Dessau and Shen (1999) estimated the exchange energy for flipping an e_g -electron to be 2.7 eV.

Okimoto et al. (1995) studying the optical spectra of $\text{La}_{1-x}\text{Sr}_x\text{MnO}_3$ with $x=0.175$ estimated the value of the Hund coupling to be of the order of 2 eV, much larger than the hopping of the one-orbital model for manganites. Note that in estimations of this variety care must be taken with the actual definition of the exchange J_H , which sometimes is in front of a ferromagnetic Heisenberg interaction where classical localized spins of module 1 are used, while in other occasions quantum spins of value $3/2$ are employed. Nevertheless, the main message of Okimoto et al.’s paper is that J_H is larger than the hopping. A reanalysis of Okimoto et al.’s results led Millis, Mueller and Shraiman (1996) to conclude that the Hund coupling is actually even larger than previously believed. The optical data of Quijada et al. (1998) and Machida et al. (1998) also suggest that the Hund coupling is larger than 1 eV. Similar conclusions were reached by Satpathy et al. (1996) using constrained LDA calculations.

The crystal-field splitting between the e_g - and t_{2g} -states was estimated to be of the order of 1 eV by Tokura (1999) (see also Yoshida, 1998). It

is clear that manganites are in high-spin ionic states due to their large Hund coupling.

Regarding the hopping “ t ”, Dessau and Shen (1999) reported a value of order 1eV, which is somewhat larger than other estimations. In fact, the results of Bocquet et al. (1992), Arima et al. (1993), and Saitoh et al. (1995) locate its magnitude between 0.2 eV and 0.5 eV, which is reasonable in transition metal oxides. However, note that fair comparisons between theory and experiment require calculations of, e.g., quasiparticle band dispersions, which are difficult at present. Nevertheless it is widely accepted that the hopping is just a fraction of eV.

Dessau and Shen (1999) estimated the static Jahn-Teller energy E_{JT} as 0.25eV. From the static Jahn-Teller energy and the hopping amplitude, it is convenient to define the dimensionless electron-phonon coupling constant λ as

$$\lambda = \sqrt{2E_{JT}/t} = g/\sqrt{k_{JT}t}. \quad (1.46)$$

By using $E_{JT}=0.25\text{eV}$ and $t=0.2\sim 0.5\text{eV}$, λ is estimated as between 1 \sim 1.6. Actually, Millis, Mueller and Shraiman (1996) concluded that λ is between 1.3 and 1.5.

As for the parameter β , it is given by $\beta=k_{br}/k_{JT}=(\omega_{br}/\omega_{JT})^2$, where ω_{br} and ω_{JT} are the vibration energies for manganite breathing- and Jahn-Teller-modes, respectively, assuming that the reduced masses for those modes are equal. From experimental results and band-calculation data (see Iliev et al. 1998), ω_{br} and ω_{JT} are estimated as $\sim 700\text{cm}^{-1}$ and $500\text{-}600\text{cm}^{-1}$, respectively, leading to $\beta\approx 2$. However, in practice it has been observed that the main conclusions are basically unchanged as long as β is larger than unity. Thus, if an explicit value for β is not provided, the reader can consider that β is simply taken to be ∞ to suppress the breathing mode distortion.

The value of J_{AF} is the smallest of the set of couplings discussed here. In units of the hopping, it is believed to be of the order of $0.1t$ (see Perring et al., 1997), namely about 200K. Note, however, that it would be a bad approximation to simply neglect this parameter since in the limit of vanishing density of e_g electrons, J_{AF} is crucial to induce antiferromagnetism, as it occurs in CaMnO_3 for instance. Its relevance, at hole densities close to 0.5 or larger, to the formation of antiferromagnetic charge-ordered states is remarked elsewhere in this chapter. Also in mean-field approximations by Maezono, Ishihara, and Nagaosa (1998) the importance of J_{AF} has been mentioned, even though in their work this coupling was estimated to be only $0.01t$.

Summarizing, it appears well-established that: (i) the largest energy scales in the Mn-oxide models studied here are the Coulomb repulsions

between electrons in the same ion, which is quite reasonable. (ii) The Hund coupling is between 1 and 2 eV, larger than the typical hopping amplitudes, and sufficiently large to form high-spin Mn^{4+} and Mn^{3+} ionic states. As discussed elsewhere in this chapter, a large J_H leads naturally to a vanishing probability of e_g -electron double-occupancy of a given orbital, thus mimicking the effect of a strong on-site Coulomb repulsion. (iii) The dimensionless electron-phonon coupling constant λ is of the order of unity, showing that the electron lattice interaction is substantial and cannot be neglected. (iv) The electron hopping energy is a fraction of eV. (v) The AF-coupling among the localized spins is about a tenth of the hopping. However, as remarked elsewhere, this apparent small coupling can be quite important in the competition between FM and AF states.

3. Spin-Charge-Orbital Ordering

In the complicated phase diagram for manganites, there appear so many magnetic phases. A key concept to classify these phases is the charge and orbital ordering. Especially, “orbital ordering” is the remarkable feature, characteristic to manganites with active e_g orbital. In this section, spin, charge, and orbital structure for the typical hole doping in the phase diagram of manganites is focused by stressing the importance of orbital ordering.

Note that the one-orbital model for manganites contains interesting physics, notably a FM-AF competition that has similarities with those found in experiments. However, it is clear that to explain the notorious orbital order tendency in Mn-oxides, it is crucial to use a model with two orbitals, and in a previous section such a model was defined for the case where there is an electron Jahn-Teller phonon coupling and also Coulomb interactions. Under the assumption that both localized t_{2g} spins and phonons are classical, the model without Coulombic terms can be studied fairly accurately using numerical and mean-field approximations. For the case where Coulomb terms are included, unfortunately, computational studies are difficult but mean-field approximations can still be carried out.

3.1 $x=0.0$

First let us consider the mother material LaMnO_3 with one e_g electron per site. This material has the insulating AF phase with A-type AF spin order, in which t_{2g} spins are ferromagnetic in the a - b plane and antiferromagnetic along the c -axis. Recent investigations by Hotta et al. (1999) have shown that, in the context of the model with Jahn-Teller

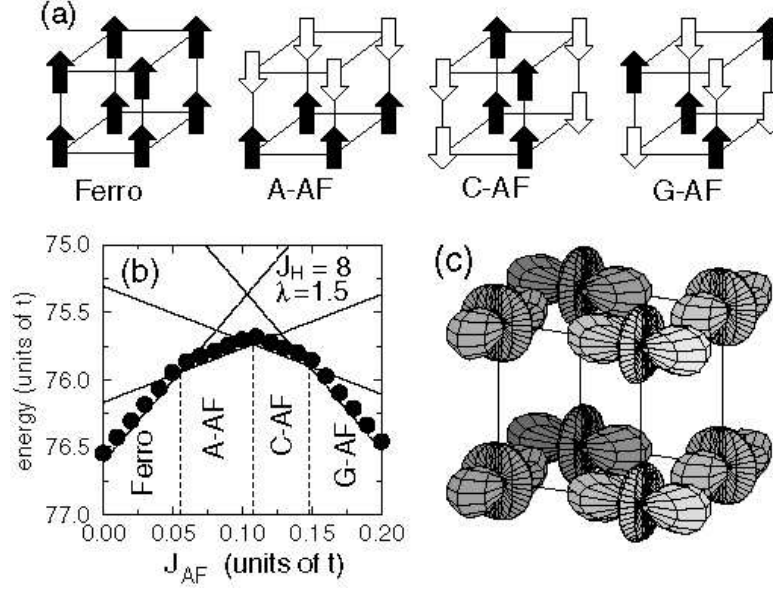


Figure 1.3. (a) The four spin arrangements for Ferro, A-AF, C-AF, and G-AF. (b) Total energy vs J_{AF} on a 2^3 cluster at low temperature with $J_H=8t$ and $\lambda=1.5$. The results were obtained using Monte Carlo and relaxational techniques, with excellent agreement among them. (c) Orbital order corresponding to the A-type AF state. For more details the reader should consult Hotta et al., 1999.

phonons, the important ingredient to understand the A-type AF phase is J_{AF} , namely by increasing this coupling from 0.05 to larger values, a transition from a FM to an A-type AF exists (the relevance of Jahn-Teller couplings at $\langle n \rangle=1.0$ has also been remarked by Capone, Feinberg, and Grilli, 2000). This can be visualized easily in Fig. 1.3, where the energy vs. J_{AF} at fixed intermediate λ and J_H is shown. Four regimes were identified: FM, A-AF, C-AF, and G-AF states that are sketched also in that figure. The reason is simple: as J_{AF} grows, the tendency toward spin AF must grow since this coupling favors such an order. If J_{AF} is very large, then it is clear that a G-AF state must be the one that lowers the energy, in agreement with the Monte Carlo simulations. If J_{AF} is small or zero, there is no reason why spin AF will be favorable at intermediate λ and the density under consideration, and then the state is ferromagnetic to improve the electronic mobility. It should be no surprise that at intermediate J_{AF} , the dominant state is intermediate between the two extremes, with A-type and C-type antiferromagnetism becoming stable in intermediate regions of parameter space.

It is interesting to note that similar results regarding the relevance of J_{AF} to stabilize the A-type order have been found by Koshibae et al. (1997) in a model with Coulomb interactions. An analogous conclusion was found by Solov'yev, Hamada, and Terakura (1996) and Ishihara et al. (1997). Betouras and Fujimoto (1999), using bosonization techniques for the one-dimensional one-orbital model, also emphasized the importance of J_{AF} , similarly as did Yi, Yu, and Lee (1999) based on Monte Carlo studies in two dimensions of the same model. The overall conclusion is that there are clear analogies between the strong Coulomb and strong Jahn-Teller coupling approaches, as discussed elsewhere in this chapter. Actually in the mean-field approximation, it was shown by Hotta, Malvezzi, and Dagotto (2000) that the influence of the Coulombic terms can be hidden in simple redefinitions of the electron-phonon couplings (see also Benedetti and Zeyher, 1999). In our opinion, both approaches (Jahn-Teller and Coulomb) have strong similarities and it is not surprising that basically the same physics is obtained in both cases. Actually, Fig. 2 of Maezono, Ishihara, and Nagaosa (1998) showing the energy vs. J_{AF} in mean-field calculations of the Coulombic Hamiltonian without phonons is very similar to our Fig. 1.3, aside from overall scales. On the other hand, Mizokawa and Fujimori (1995, 1996) states that the A-type AF is stabilized only when the Jahn-Teller distortion is included, namely, the FM phase is stabilized in the purely Coulomb model, based on the unrestricted Hartree-Fock calculation for the $d-p$ model.

The issue of what kind of orbital order is concomitant with A-type AF order is an important matter. This has been discussed at length by Hotta et al. (1999), and the final conclusion, after the introduction of perturbations caused by the experimentally known difference in lattice spacings between the three axes, is that the order shown in Fig. 1.3(c) minimizes the energy. This state has indeed been identified in recent x-ray experiments, and it is quite remarkable that such a complex pattern of spin and orbital degrees of freedom indeed emerges from mean-field and computational studies. Studies by van den Brink et al. (1998) using purely Coulombic models arrived at similar conclusions.

Why does the orbital order occur here? This can be easily understood perturbatively in the hopping t . A hopping matrix only connecting the same orbitals, with hopping parameter t , is assumed for simplicity. The energy difference between e_g orbitals at a given site is E_{JT} , which is a monotonous function of λ . For simplicity, in the notation let us refer to orbital uniform (staggered) as orbital “FM” (“AF”). Case (a) corresponds to spin FM and orbital AF: In this case when an electron moves from orbital a on the left to the same orbital on the right, which is the only possible hopping by assumption, an energy of order E_{JT} is

lost, but kinetic energy is gained. As in any second order perturbative calculation the energy gain is then proportional to t^2/E_{JT} . In case (b), both spin and orbital FM, the electrons do not move and the energy gain is zero (again, the nondiagonal hoppings are assumed negligible just for simplicity). In case (c), the spin are AF but the orbitals are FM. This is like a one orbital model and the gain in energy is proportional to $t^2/(2J_H)$. Finally, in case (d) with AF in spin and orbital, both Hund and orbital splitting energies are lost in the intermediate state, and the overall gain becomes proportional to $t^2/(2J_H + E_{JT})$. As a consequence, if the Hund coupling is larger than E_{JT} , then case (a) is the best, as it occurs at intermediate E_{JT} values. Then, the presence of orbital order can be easily understood from a perturbative estimation, quite similarly as done by Kugel and Khomskii (1974) in their pioneering work on orbital order.

Finally let us provide a comment on the FM tendency at $x=0.0$. Carrying out Monte Carlo simulations in the localized spins and phonons, and considering exactly the electrons in the absence of an explicit Coulomb repulsion, a variety of correlations have been calculated to establish the $\langle n \rangle=1.0$ phase diagram. Typical results for the spin and orbital structure factors, $S(q)$ and $T(q)$ respectively, were presented by Yunoki et al. (1998b). At small λ , $S(0)$ is dominant and $T(q)$ is not active. This signals a ferromagnetic state with disordered orbitals, namely a standard ferromagnet (note, however, that van den Brink and Khomskii (2001) and Maezono and Nagaosa (2000) believe that this state in experiments may have complex orbital ordering). The result with FM tendencies dominating may naively seem strange given the fact that for the one-orbital model at $\langle n \rangle=1.0$ an AF state was found. But here two orbitals are being considered and one electron per site is 1/2 electron per orbital. In this respect, $\langle n \rangle=1.0$ with two orbitals should be similar to $\langle n \rangle=0.5$ for one orbital and indeed in the last case a ferromagnetic state was observed.

3.2 $x=0.5$

Now let us move to another important doping $x=0.5$. For half-doped perovskite manganites, the so-called CE-type AFM phase has been established as the ground state in the 1950's. This phase is composed of zigzag FM arrays of t_{2g} -spins, which are coupled antiferromagnetically perpendicular to the zigzag direction. Furthermore, the checkerboard-type charge ordering in the x - y plane, the charge stacking along the z -axis, and $(3x^2 - r^2/3y^2 - r^2)$ orbital ordering are associated with this phase. A schematic view of CE-type structure is shown in Fig. 1.4(a).

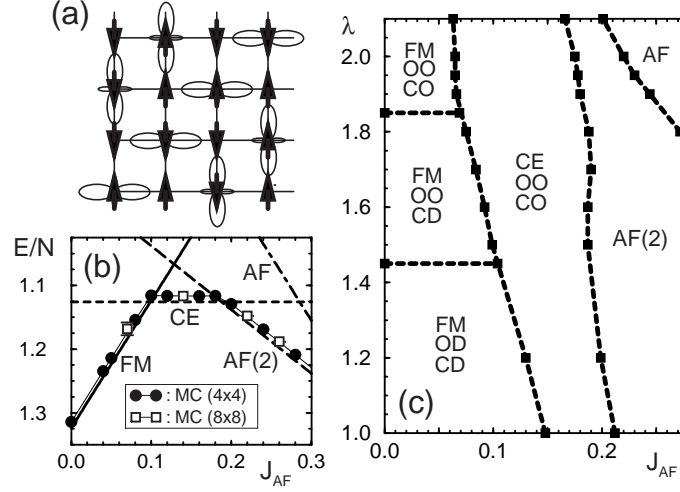


Figure 1.4. (a) Schematic view of CE-type structure at $x=0.5$. (b) Monte Carlo energy per site vs J_{AF} at density $x=0.5$, $\lambda=1.5$, low temperature $T=1/100$, and $J_H=\infty$, using the two-orbital model in two dimensions with Jahn-Teller phonons (non-cooperative ones). FM, CE, and AF states were identified measuring charge, spin, and orbital correlations. “AF(2)” denotes a state with spins $\uparrow\uparrow\downarrow\downarrow$ in one direction, and antiferromagnetically coupled in the other. The clusters used are indicated. (c) Phase diagram in the plane λ - J_{AF} at $x=0.5$, obtained numerically using up to 8×8 clusters. All transitions are of first-order. The notation is the standard one (CD = charge disorder, CO = charge order, OO = orbital order, OD = orbital disorder). Results reproduced from Yunoki, Hotta and Dagotto (2000), where more details can be found.

Although there is little doubt that the famous CE-state of Goodenough is indeed the ground state of $x=0.5$ intermediate and low bandwidth manganites, only very recently such a state has received theoretical confirmation using unbiased techniques, at least within some models. In the early approach of Goodenough it was *assumed* that the charge was distributed in a checkerboard pattern, upon which spin and orbital order was found. But it would be desirable to obtain the CE-state based entirely upon a more fundamental theoretical analysis, as the true state of minimum energy of a well-defined and realistic Hamiltonian. If such a calculation can be done, as a bonus one would find out which states compete with the CE-state in parameter space, an issue very important in view of the mixed-phase tendencies of Mn-oxides, which cannot be handled within the approach of Goodenough.

One may naively believe that it is as easy as introducing a huge nearest-neighbor Coulomb repulsion V to stabilize a charge-ordered state at $x=0.5$, upon which the reasoning of Goodenough can be applied. How-

ever, there are at least two problems with this approach. First, such a large V quite likely will destabilize the ferromagnetic charge-disordered state and others supposed to be competing with the CE-state. It may be possible to explain the CE-state with this approach, but not others also observed at $x=0.5$ in large bandwidth Mn-oxides. Second, a large V would produce a checkerboard pattern in the *three* directions. However, experimentally it has been known for a long time (Wollan and Koehler, 1955) that the charge *stacks* along the z -axis, namely the same checkerboard pattern is repeated along z , rather than being shifted by one lattice spacing from plane to plane. A dominant Coulomb interaction V can not be the whole story for $x=0.5$ low-bandwidth manganese oxides.

The nontrivial task of finding a CE-state with charge stacked along the z -axis without the use of a huge nearest-neighbors repulsion has been recently performed by Yunoki, Hotta, and Dagotto (2000) using the two-orbital model with strong electron Jahn-Teller phonon coupling. The calculation proceeded using an unbiased Monte Carlo simulation, and as an output of the study, the CE-state indeed emerged as the ground-state in some region of coupling space. Typical results are shown in Figs. 1.4(b) and (c). In part (b) the energy at very low temperature is shown as a function of J_{AF} at fixed density $x=0.5$, $J_H=\infty$ for simplicity, and with a robust electron-phonon coupling $\lambda=1.5$ using the two orbital model H_{JT} . At small J_{AF} , a ferromagnetic phase was found to be stabilized, according to the Monte Carlo simulation. Actually, at $J_{AF}=0.0$ it has not been possible to stabilize a partially AF-state at $x=0.5$, namely the states are always ferromagnetic at least within the wide range of λ 's investigated (but they can have charge and orbital order). On the other hand, as J_{AF} grows, a tendency to form AF links develops, as it happens at $x=0.0$. At large J_{AF} eventually the system transitions to states that are mostly antiferromagnetic, such as the so-called “AF(2)” state of Fig. 1.4(b) (with an up-up-down-down spin pattern repeated along one axis, and AF coupling along the other axis), or directly a fully AF-state in both directions.

However, the intermediate values of J_{AF} are the most interesting ones. In this case the energy of the two-dimensional clusters become flat as a function of J_{AF} suggesting that the state has the same number of FM and AF links, a property that the CE-state indeed has. By measuring charge-correlations it was found that a checkerboard pattern is formed particularly at intermediate and large λ 's, as in the CE-state. Finally, after measuring the spin and orbital correlations, it was confirmed that indeed the complex pattern of the CE-state was fully stabilized in the simulation. This occurs in a robust portion of the λ - J_{AF} plane, as shown

in Fig. 1.4(c). The use of J_{AF} as the natural parameter to vary in order to understand the CE-state is justified based on Fig. 1.4, since the region of stability of the CE-phase is elongated along the λ -axis, meaning that its existence is not so much dependent on that coupling but much more on J_{AF} itself. It appears that some explicit tendency in the Hamiltonian toward the formation of AF links is necessary to form the CE-state. If this tendency is absent, a FM state is formed, while if it is too strong an AF-state appears. The $x=0.5$ CE-state, similar to the A-type AF at $x=0.0$, needs an intermediate value of J_{AF} for stabilization. The stability window is finite and in this respect there is no need to carry out a *fine* tuning of parameters to find the CE phase. However, it is clear that there is a balance of AF and FM tendencies in the CE-phase that makes the state somewhat fragile.

Note that the transitions among the many states obtained when varying J_{AF} are all of *first* order, namely they correspond to crossings of levels at zero temperature. The first-order character of these transitions is a crucial ingredient of the recent scenario proposed by Moreo et al. (2000) involving mixed-phase tendencies with coexisting clusters with *equal* density. Recently, first-order transitions have also been reported in the one-orbital model at $x=0.5$ by Alonso et al. (2001a, 2001b), as well as tendencies toward phase separation. Recent progress in the development of powerful techniques for manganite models (Alonso et al., 2001c; Motome and Furukawa, 1999, 2000) will contribute to the clarification of these issues in the near future.

Let us address now the issue of charge-stacking (CS) along the z -axis. For this purpose simulations using three-dimensional clusters were carried out. The result for the energy vs. J_{AF} is shown in Fig. 1.5(a), with $J_H=\infty$ and $\lambda=1.6$ fixed. The CE-state with charge-stacking has been found to be the ground state on a wide J_{AF} window. The reason that this state has lower energy than the so-called “Wigner-crystal” (WC) version of the CE-state, namely with the charge spread as much as possible, is once again the influence of J_{AF} . With a charge stacked arrangement, the links along the z -axis can all be simultaneously antiferromagnetic, thereby minimizing the energy. In the WC-state this is not possible.

It should be noted that this charge stacked CE-state is not immediately destroyed when the weak nearest-neighbor repulsion V is introduced to the model, as shown in Fig. 1.5(b), obtained in the mean-field calculations by Hotta, Malvezzi, and Dagotto (2000). If V is further increased for a realistic value of J_{AF} , the ground state eventually changes from the charge stacked CE-phase to the WC version of the CE-state or the C-type AFM phase with WC charge ordering. As explained above, the stability of the charge stacked phase to the WC version of the CE-

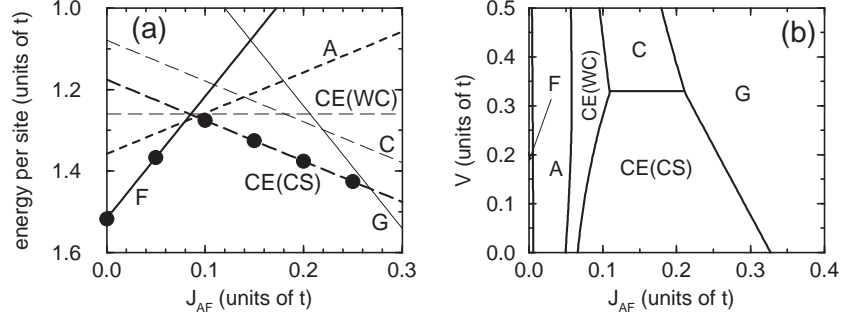


Figure 1.5. (a) Energy per site as a function of J_{AF} for $\lambda=1.6$ and $J_H=\infty$ for H_{JT} . The curves denote the mean-field results and the solid symbols indicate the energy obtained by the relaxation method. Thick solid, thick broken, thin broken, thick dashed, thin dashed, thin broken, and thin solid lines denotes FM, A-type, CE-type with WC structure, charge-stacked CE-type, C-type, and G-type states, respectively. Note that the charge-stacked CE-state is observed in experiments. (d) Phase diagram in the (J_{AF}, V) plane. Note that the charge-stacked structure along the z -axis can be observed only in the CE-type AFM phase. Results reproduced from Hotta, Malvezzi, and Dagotto (2000), where more details can be found.

state is due to the magnetic energy difference. However, the competition between the charge-stacked CE-state and the C-type AFM phase with the WC structure is not simply understood by the effect of J_{AF} , since those two kinds of AFM phases have the same magnetic energy. In this case, the stabilization of the charge stacking originates from the difference in the geometry of the one-dimensional FM path, namely a zigzag-path for the CE-phase and a straight-line path for the C-type AFM state. As will be discussed later, the energy for e_g electrons in the zigzag path is lower than that in the straight-line path, and this energy difference causes the stabilization of the charge stacking. In short, the stability of the charge-stacked structure at the expense of V is supported by “the geometric energy” as well as the magnetic energy. Note that each energy gain is just a fraction of t . Thus, in the absence of other mechanisms to understand the charge-stacking, another consequence of this analysis is that V actually must be substantially *smaller* than naively expected, otherwise such a charge pattern would not be stable. In fact, estimations given by Yunoki, Hotta, and Dagotto (2000) suggest that the manganites must have a large dielectric function at short distances (see Arima and Tokura, 1995) to prevent the melting of the charge-stacked state.

Note also that the mean-field approximations by Hotta, Malvezzi, and Dagotto (2000) have shown that on-site Coulomb interactions U and U' can *also* generate a two-dimensional CE-state, in agreement with

the calculations by van den Brink et al. (1999). Then, the present authors believe that strong Jahn-Teller and Coulomb couplings tend to give similar results. This belief finds partial confirmation in the mean-field approximations of Hotta, Malvezzi, and Dagotto (2000), where the similarities between a strong λ and (U, U') were investigated. Even doing the calculation with Coulombic interactions, the influence of J_{AF} is still crucial to inducing charge-stacking (note that the importance of this parameter has also been recently remarked by Mathieu, Svedlindh and Nordblad, 2000, based on experimental results).

Many other authors carried out important work in the context of the CE-state at $x=0.5$. For example, with the help of Hartree-Fock calculations, Mizokawa and Fujimori (1997) reported the stabilization of the CE-state at $x=0.5$ only if Jahn-Teller distortions were incorporated into a model with Coulomb interactions. This state was found to be in competition with a uniform FM state, as well as with an A-type AF-state with uniform orbital order. In this respect the results are very similar to those found by Yunoki, Hotta and Dagotto (2000) using Monte Carlo simulations. In addition, using a large nearest neighbor repulsion and the one-orbital model, charge ordering and a spin structure compatible with the zigzag chains of the CE state was found by Lee and Min (1997) at $x=0.5$. Also Jackeli et al. (1999) obtained charge-ordering at $x=0.5$ using mean-field approximations and a large V . Charge-stacking was not investigated by those authors. The CE-state in $x=0.5$ $\text{Pr}_{1-x}\text{Ca}_x\text{MnO}_3$ was also obtained by Anisimov et al. (1997) using LSDA+U techniques.

3.3 $x > 0.5$

In the previous subsection, the discussion focused on the CE-type AFM phase at $x=0.5$. Naively, it may be expected that similar arguments can be extended to the regime $x > 1/2$, since in the phase diagram for $\text{La}_{1-x}\text{Ca}_x\text{MnO}_3$, the AFM phase has been found at low temperatures in the region $0.50 < x < 0.88$. Then, let us try to consider the band-insulating phase for density $x=2/3$ based on H^∞ , without both the Jahn-Teller phononic and Coulombic interactions, since this doping is quite important for the appearance of the bi-stripe structure (see Mori et al., 1998).

After several calculations for $x=2/3$, as reported by Hotta et al. (2000), the lowest-energy state was found to be characterized by the straight path, not the zigzag one, leading to the C-type AFM phase which was also discussed in previous Sections. For a visual representation of the C-type state, see Fig. 4 of Kajimoto et al., 1999. At first glance, the zigzag structure similar to that for $x=0.5$ could be the ground-state for the same reason as it occurs in the case of $x=0.5$. However, while it

is true that the state with such a zigzag structure is a band-insulator, the energy gain due to the opening of the bandgap is not always the dominant effect. In fact, even in the case of $x=0.5$, the energy of the bottom of the band for the straight path is $-2t_0$, while for the zigzag path, it is $-\sqrt{3}t_0$. For $x=1/2$, the energy gain due to the gap opening overcomes the energy difference at the bottom of the band, leading to the band-insulating ground-state. However, for $x=2/3$ even if a band-gap opens the energy of the zigzag structure cannot be lower than that of the metallic straight-line phase. Intuitively, this point can be understood as follows: An electron can move smoothly along the one-dimensional path if it is straight. However, if the path is zigzag, “reflection” of the wavefunction occurs at the corner, and then a smooth movement of one electron is no longer possible. Thus, for small numbers of carriers, it is natural that the ground-state is characterized by the straight path to optimize the kinetic energy of the e_g electrons.

However, in neutron scattering experiments a spin pattern similar to the CE-type AFM phase has been suggested (Radaelli et al., 1999). In order to stabilize the zigzag AFM phase to reproduce those experiments it is necessary to include the Jahn-Teller distortion effectively. As discussed in Hotta et al. (2000), a variety of zigzag paths could be stabilized when the Jahn-Teller phonons are included. In such a case, the classification of zigzag paths is an important issue to understand the competing “bi-stripe” vs. “Wigner-crystal” structures. The former has been proposed by Mori et al. (1998), while the latter was claimed to be stable by Radaelli et al. (1999). In the scenario by Hotta et al. (2000), the shape of the zigzag structure is characterized by the “winding number” w associated with the Berry-phase connection of an e_g -electron parallel-transported through Jahn-Teller centers, along zigzag one-dimensional paths. Namely, it is defined as

$$w = \oint \frac{d\mathbf{r}}{2\pi} \nabla \xi. \quad (1.47)$$

This quantity has been proven to be an integer, which is a topological invariant (See Hotta et al., 1998. See also Koizumi et al., 1998a and 1998b). Note that the integral indicates an accumulation of the phase difference along the one-dimensional FM path in the unit length. This quantity is equal to half of the number of corners included in the unit path, which can be shown as follows. The orbital polarizes along the hopping direction, indicating that $\xi_i=2\pi/3$ ($4\pi/3$) along the x -(y -)direction, as was pointed out above. This is simply the double exchange mechanism in the orbital degree of freedom. Thus, the phase does not change in the straight segment part, indicating that $w=0$ for the straight-line

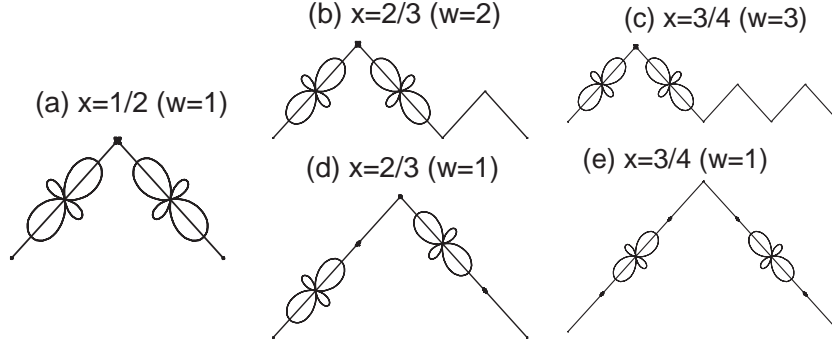


Figure 1.6. (a) Path with $w=1$ at $x=1/2$. Charge and orbital densities are calculated in the MFA for $E_{JT}=2t$. At each site, the orbital shape is shown with its size in proportion to the orbital density. (b) The BS-structure path with $w=2$ at $x=2/3$. (c) The BS-structure path with $w=3$ at $x=3/4$. (d) The WC-structure path with $w=1$ at $x=2/3$. (e) The WC-structure path with $w=1$ at $x=3/4$.

path. However, when an e_g -electron passes a corner site, the hopping direction is changed, indicating that the phase change occurs at that corner. When the same e_g -electron passes the next corner, the hopping direction is again changed. Then, the phase change in ξ_i after moving through a couple of corners should be 2π , leading to an increase of unity in w . Thus, the total winding number is equal to half of the number of corners included in the zigzag unit path. Namely, the winding number w is a good label to specify the shape of the zigzag one-dimensional FM path.

After several attempts to include effectively the Jahn-Teller phonons, it was found that the bi-stripe phase and the Wigner crystal phase universally appear for $w=x/(1-x)$ and $w=1$, respectively. Note here that the winding number for the bi-stripe structure has a remarkable dependence on x , reflecting the fact that the distance between adjacent bi-stripes changes with x . This x -dependence of the modulation vector of the lattice distortion has been observed in electron microscopy experiments (Mori et al., 1998). The corresponding zigzag paths with the charge and orbital ordering are shown in Fig. 1.6. In the bi-stripe structure, the charge is confined in the short straight segment as in the case of the CE-type structure at $x=0.5$. On the other hand, in the Wigner-crystal structure, the straight segment includes two sites, indicating that the charge prefers to occupy either of these sites. Then, to minimize the Jahn-Teller energy and/or the Coulomb repulsion, the e_g electrons are distributed with equal spacing. The corresponding spin structure is shown in Fig. 1.7. A difference in the zigzag geometry can

produce a significant different in the spin structure. Following the definitions for the C- and E-type AFM structures (see Wollan and Koehler, 1955), the bi-stripe and Wigner crystal structure have $C_{1-x}E_x$ -type and C_xE_{1-x} -type AFM spin arrangements, respectively. Note that at $x=1/2$, half of the plane is filled by the C-type, while another half is covered by the E-type, clearly illustrating the meaning of “CE” in the spin structure of half-doped manganites.

The charge structure along the z -axis for $x=2/3$ has been discussed by Hotta et al. (2000), as schematically shown in Figs. 1.7(e) and (f), a remarkable feature can be observed. Due to the confinement of charge in the short straight segment for the bi-stripe phase, the charge stacking is suggested from our topological argument. On the other hand, in the Wigner-crystal type structure, charge is not stacked, but it is shifted by one lattice constant to avoid the Coulomb repulsion. Thus, if the charge stacking is also observed in the experiment for $x=2/3$, our topological scenario suggests the bi-stripe phase as the ground-state in the low temperature region. To firmly establish the final “winner” in the competition between the bi-stripe and Wigner-crystal structure at $x=2/3$, more precise experiments, as well as quantitative calculations, will be needed in the future.

3.4 $x < 0.5$

Regarding densities smaller than 0.5, the states at $x=1/8$, $1/4$ and $3/8$ have received considerable attention recently (see Mizokawa et al., 2000; Korotin et al., 1999; Hotta and Dagotto, 2000). These investigations are still in a “fluid” state, and the experiments are not quite decisive yet, and for this reason, this issue will not be discussed in much detail here. However, without a doubt, it is very important to clarify the structure of charge-ordered states that may be in competition with the ferromagnetic states in the range in which the latter is stable in some compounds. “Stripes” may emerge from this picture, as recently remarked in experiments (Adams et al., 2000; Dai et al., 2000; Kubota et al., 2000. See also Vasiliu-Doloc et al., 1999) and calculations (Hotta, Feiguin, and Dagotto, 2000), and surely the identification of charge/orbital arrangements at $x < 0.5$ will be an important area of investigations in the very near future.

Here a typical result for this stripe-like charge ordering is shown in Fig. 1.8, in which the lower-energy orbital at each site is depicted, and its size is in proportion to the electron density occupying that orbital. This pattern is theoretically obtained by the relaxation technique for the optimization of oxygen positions, namely including the cooperative Jahn-Teller effect. At least in the strong electron-phonon coupling re-

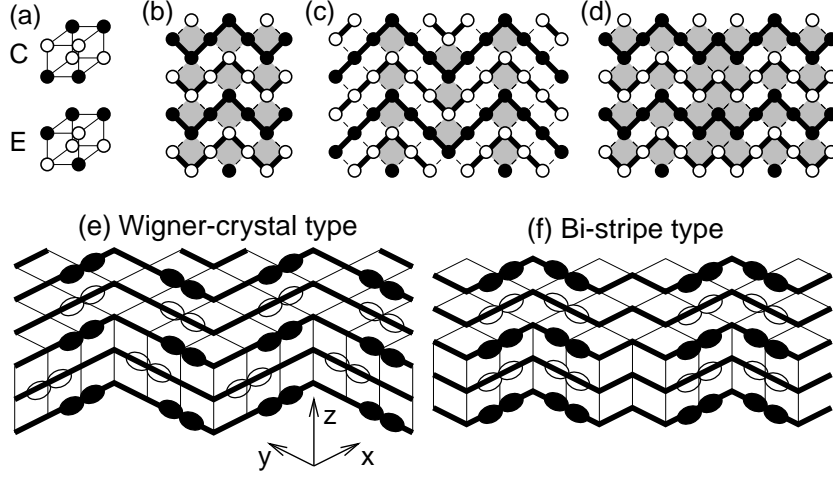


Figure 1.7. (a) C- and E-type unit cell (Wollan and Koehler, 1955). (b) The spin structure in the a - b plane at $x=1/2$. Open and solid circle denote the spin up and down, respectively. The thick line indicates the zigzag FM path. The open and shaded squares denote the C- and E-type unit cells. At $x=1/2$, C-type unit cell occupies half of the two-dimensional plane, clearly indicating the “CE” type phase. (c) The spin structure at $x=2/3$ for Wigner-crystal type phase. Note that 66% of the two-dimensional lattice is occupied by C-type unit cell. Thus, it is called “C₂E”-type AFM phase. (d) The spin structure at $x=2/3$ for bi-stripe type phase. Note that 33% of the two-dimensional lattice is occupied by C-type unit cell. Thus, it is called “CE₂”-type AFM phase. Schematic figures for spin, charge, and orbital ordering for (e) WC and (f) BS structures at $x=2/3$. The open and solid symbols indicate the spin up and down, respectively. The FM one-dimensional path is denoted by the thick line. The empty sites denote Mn⁴⁺ ions, while the robes indicate the Mn³⁺ ions in which $3x^2 - r^2$ or $3y^2 - r^2$ orbitals are occupied.

gion, the stripe charge ordering along the *diagonal* direction in the x - y plane becomes the global ground-state. Note, however, that many metastable states can appear very close to this ground state. Thus, the shape of the stripe is considered to fluctuate both in space and time, and in experiments it may occur that only some fragments of this stripe can be detected. It should also be emphasized that the orbital ordering occurs concomitant with this stripe charge ordering. In the electron-rich region, the same antiferro orbital-order exists as that corresponding to $x=0.0$. On the other hand, the pattern around the diagonal array of electron-poor sites is quite similar to the building block of the charge/orbital structure at $x=0.5$.

If these figures are rotated by 45 degrees, the same charge and orbital structure is found to stack along the b -axis. Namely, it is possible to cover the whole two-dimensional plane by some periodic charge-orbital array

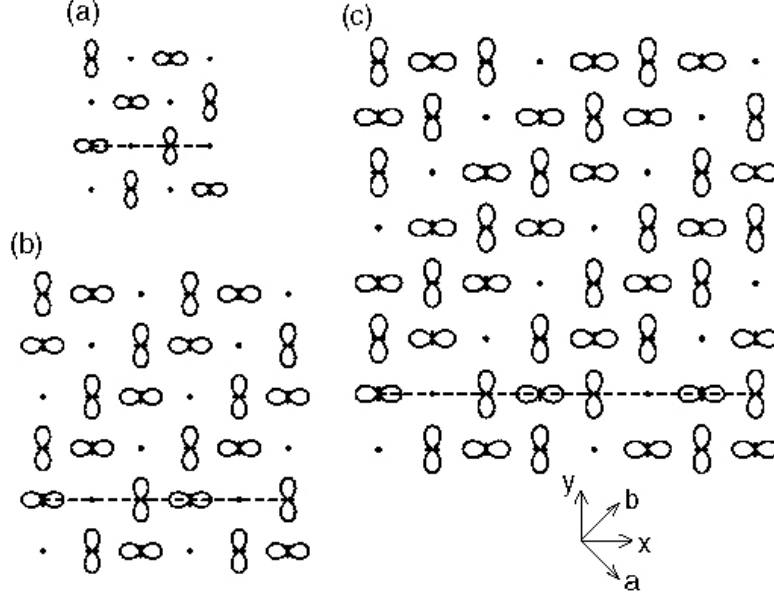


Figure 1.8. Orbital densities in the FM phase for (a) $x=1/2$, (b) $1/3$, and (c) $1/4$. The charge density in the lower-energy orbital is shown, and the size of the orbital is in proportion to this density. The broken line indicates one of the periodic paths to cover the whole two-dimensional plane.

along the a -axis (see, for instance, the broken-line path). If this periodic array is taken as the closed loop C in Eq. (1.47), the winding numbers are $w=1, 2$, and 3 , for $x=1/2, 1/3$, and $1/4$, respectively. Note that in this case w is independent of the path along the a -axis. The results imply a general relation $w=(1-x)/x$ for the charge-orbital stripe in the FM phase, reflecting the fact that the distance between the diagonal arrays of holes changes with x . Our topological argument predicts stable charge-orbital stripes at special doping such as $x=1/(1+w)$, with w an integer.

This orbital ordering can be also interpreted as providing a “ π ”-shift in the orbital sector, by analogy with the dynamical stripes found in cuprates (see, for instance, Buhler et al., 2000), although in copper oxides the charge/spin stripes mainly appear along the x - or y -directions. The study of the similarities and differences between stripes in manganites and cuprates is one of the most interesting open problems in the study of transition metal oxides, and considerable work is expected in the near future.

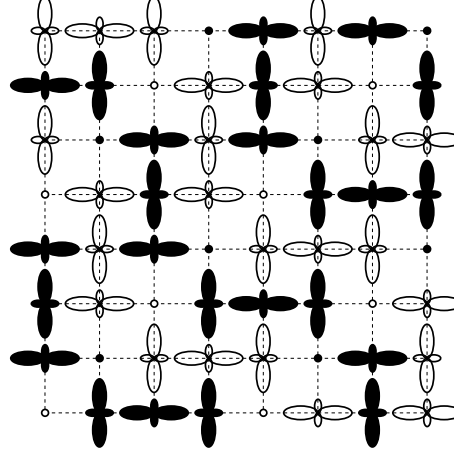


Figure 1.9. Schematic figure of the spin-charge-orbital structure at $x=1/4$ in the zigzag AFM phase at low temperature and large electron-phonon coupling. The symbol convention is the same as in Fig. 1.7. This figure was obtained using numerical techniques, and *cooperative* phonons, for $J_H=\infty$ and $J_{AF}=0.1t$. For the non-cooperative phonons, basically the same pattern can be obtained.

Finally, a new zigzag AFM spin configuration for $x<0.5$ is here briefly discussed (Hotta, Feiguin, and Dagotto, 2000). In Fig. 1.9, a schematic view of this novel spin-charge-orbital structure on the 8×8 lattice at $x=1/4$ is shown, deduced using the numerical relaxation technique applied to cooperative Jahn-Teller phonons in the strong-coupling region. This structure appears to be the global ground state, but many excited states with different spin and charge structures are also found with small excitation energy, suggesting that the AFM spin structure for $x<0.5$ in the layered manganites is easily disordered due to this “quasi-degeneracy” in the ground state. This result may be related to the “spin-glass” nature of the single layer manganites reported in experiments (see Moritomo et al., 1995).

It should be noted that the charge-orbital structure is essentially the same as that in the two-dimensional FM phase (see Fig. 1.9). This suggests the following scenario for the layered manganites: When the temperature is decreased from the higher temperature region, first charge ordering occurs due to the cooperative Jahn-Teller distortions in the FM (or paramagnetic) region. If the temperature is further decreased, the zigzag AFM spin arrangement is stabilized, adjusting itself to the orbital structure. Thus, the separation between the charge ordering temperature T_{CO} and the Néel temperature T_N occurs naturally in this context. This is not surprising, since T_{CO} is due to the electron-lattice coupling,

while T_N originates in the coupling J_{AF} . However, if the electron-phonon coupling is weak, then T_{CO} becomes very low. In this case, the transition to the zigzag AFM phase may occur prior to the charge ordering. As discussed above, the e_g electron hopping is confined to one dimensional structures in the zigzag AFM environment. Thus, in this situation, even a weak coupling electron-phonon coupling can produce the charge-orbital ordering, as easily understood from the Peierls instability argument. Namely, just at the transition to the zigzag AFM phase, the charge-orbital ordering occurs simultaneously, indicating that $T_{CO}=T_N$. Note also that in the zigzag AFM phase, there is no essential difference in the charge-orbital structures for the non-cooperative and cooperative phonons, due to the one-dimensionality of those zigzag chains.

3.5 Orbital ordering in related material

In previous sections the charge and orbital ordering has been discussed in detail for manganites, but recently it has been widely recognized that orbital ordering is ubiquitous in transition metal oxides and f-electron systems. Among them an importance of hidden orbital ordering has been suggested in the single-layered ruthenate by Hotta and Dagotto (2001). As is well known, Sr_2RuO_4 is triplet superconductor (see Maeno, Rice, and Sigrist, 2001). When Sr is partially substituted by Ca, superconductivity is rapidly destroyed and a paramagnetic metallic phase appears, while for $\text{Ca}_{1.5}\text{Sr}_{0.5}\text{RuO}_4$, a nearly FM metallic phase has been suggested. Upon further substitution, the system eventually transforms into an AFM insulator (Nakatsuji and Maeno, 2000). The G-type AFM phase in Ca_2RuO_4 is characterized as a standard Néel state with spin $S=1$ (Nakatsuji et al., 1997 and Braden et al., 1998). To understand the Néel state observed in experiments, one may consider the effect of the tetragonal crystal field, leading to the splitting between xy and {yz,zx} orbitals, where the xy-orbital state is lower in energy than the other levels. When the xy-orbital is fully occupied, a simple superexchange interaction at strong Hund coupling can stabilize the AFM state. However, recent X-ray absorption spectroscopy studies have shown that 0.5 holes per site exist in the xy-orbital, while 1.5 holes are contained in the zx- and yz-orbitals (Mizokawa et al., 2001), suggesting that the above naive picture based on crystal field effects is incomplete. This fact suggests that the orbital degree of freedom may play a more crucial role in the magnetic ordering in ruthenates than previously anticipated.

In order to understand the G-AFM phase with peculiar hole arrangement, the 3-orbital (t_{2g}) Hubbard model tightly coupled to lattice distortions has been analyzed using numerical and mean-field techniques (Hotta and Dagotto, 2001). Note here that Ru^{4+} ion takes the low

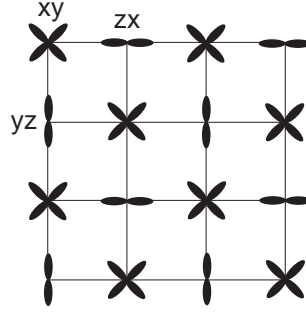


Figure 1.10. Schematic view of orbital ordering pattern proposed for the G-type AFM phase of Ca_2RuO_4 .

spin state, in which four electrons occupy t_{2g} orbital. Since this model includes several degrees of freedom, namely 2-spin and 3-orbital per electron, it is quite difficult to study large-size clusters. However, it is believed that the essential character of the competing states can be captured using a small cluster, through the combination of the Lanczos method and relaxational techniques. Mean-field approximations complement and support the results obtained numerically. An important conclusion of this analysis is that the G-type AFM phase is stabilized only when *both* Coulombic and phononic interactions are taken into account. The existence of a novel orbital ordering (see Fig. 1.10) is crucial to reproduce the peculiar hole arrangement observed in experiments by Mizokawa et al., 2001. Another interesting consequence of this study is the possibility of large magneto-resistance phenomena in ruthenates, since in our phase diagram the “metallic” FM phase is adjacent to the “insulating” AFM state. This two-phase competition is at the heart of CMR in manganites, as has been emphasized in this chapter, and thus, CMR-like phenomenon could also exist in ruthenates. For more details the reader should consult Hotta and Dagotto, 2001.

4. Phase-separation scenario

4.1 Phase Diagram with Classical Localized Spins

Although the one-orbital model for manganites is clearly incomplete to describe these compounds since, by definition, it has only one active orbital, nevertheless it has been shown in recent calculations that it captures part of the interesting competition between ferromagnetic and antiferromagnetic phases in these compounds (see, for instance, Moreo et al., 1999a). For this reason, and since this model is far simpler than the more realistic two-orbital model, it is useful to study it in detail.

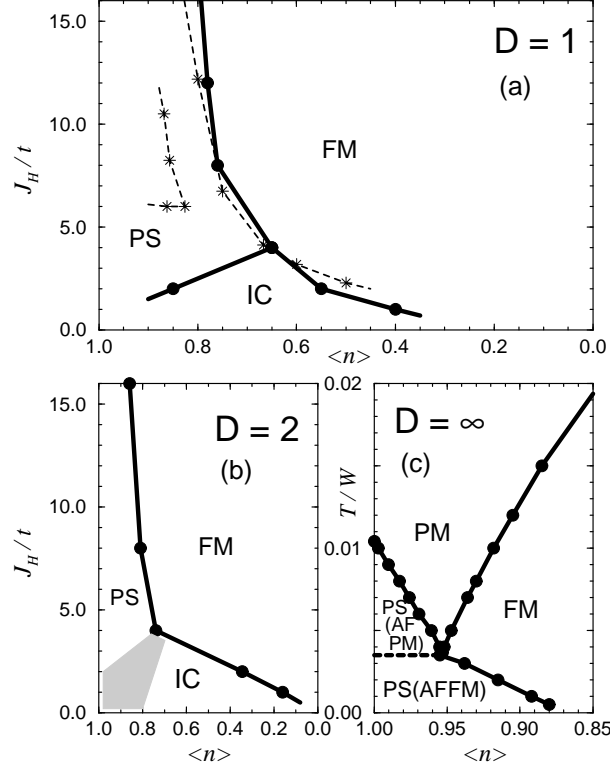


Figure 1.11. Phase diagram of the one-orbital model with classical spins (and without J_{AF} coupling). (a) are results obtained with Monte Carlo methods at low temperature in 1D (Yunoki et al., 1998a; Dagotto et al., 1998). FM, PS, and IC, denote ferromagnetic, phase-separated, and spin incommensurate phases, respectively. Although not shown explicitly, the $\langle n \rangle = 1.0$ axis is antiferromagnetic. The dashed lines correspond to results obtained using quantum localized spins. For more details see Yunoki et al. (1998a) and Dagotto et al. (1998). (b) Similar to (a) but in 2D. The grey region denotes the possible location of the PS-IC transition at low Hund coupling, which is difficult to determine. Details can be found in Yunoki et al. (1998a). (c) Results obtained in the infinite dimension limit and at large Hund coupling varying the temperature (here in units of the half-width W of the density of states). Two regions with PS were identified, as well as a paramagnetic PM regime. For details see Yunoki et al. (1998a).

A fairly detailed analysis of the phase diagram of the one-orbital model has been recently presented, mainly using computational techniques. Typical results obtained in Yunoki et al. (1998a) are shown in Fig. 1.11(a)-(c) for $D=1, 2$, and ∞ (D is spatial dimension), the first two obtained with Monte Carlo techniques at low temperature, and the third with the dynamical mean-field approximation in the large J_H limit

varying temperature. There are several important features in the results which are common in all dimensions. At e_g -density $\langle n \rangle = 1.0$, the system is antiferromagnetic (although this is not clearly shown in Fig. 1.11). The reason is that at large Hund coupling, double occupancy in the ground state is negligible at e_g -density $\langle n \rangle = 1.0$ or lower, and at these densities it is energetically better to have nearest-neighbor spins antiparallel, gaining an energy of order t^2/J_H , rather than to align them, since in such a case the system is basically frozen due to the Pauli principle. On the other hand, at finite hole density, antiferromagnetism is replaced by the tendency of holes to polarize the spin background to improve their kinetic energy. Then, a very prominent ferromagnetic phase develops in the model as shown in Fig. 1.11. This FM tendency appears in all dimensions of interest, and it manifests itself in the Monte Carlo simulations through the rapid growth with decreasing temperature, and/or increasing number of sites, of the zero-momentum spin-spin correlation, as shown by Yunoki et al. (1998a). In real space, the results correspond to spin correlations between two sites at a distance d which do not decay to a vanishing number as d grows, if there is long-range order (see results in Dagotto et al., 1998). In 1D, quantum fluctuations are expected to be so strong that long-range order cannot be achieved, but in this case the spin correlations still can decay slowly with distance following a power law. In practice, the tendency toward FM or AF is so strong even in 1D that issues of long-range order vs power-law decays are not of much importance for studying the dominant tendencies in the model. Nevertheless, care must be taken with these subtleties if very accurate studies are attempted in 1D.

The most novel result emerging from the computational studies of the one-orbital model is the way in which the FM phase is reached by hole doping of the AF phase at $\langle n \rangle = 1.0$. As explained before, mean-field approximations by de Gennes (1960) suggested that this interpolation should proceed through a so-called “canted” state in which the spin structure remains antiferromagnetic in two directions but develops a uniform moment along the third direction. For many years this canted state was assumed to be correct, and many experiments were analyzed based on such state. However, the computational studies showed that instead of a canted state, an electronic “phase separated” (PS) regime interpolates between the FM and AF phases. This PS region is very prominent in the phase diagram of Fig. 1.11(a)-(c) in all dimensions.

As an example of how PS is obtained from the computational work, consider Fig. 1.12. In the Monte Carlo simulations carried out in this context, performed in the grand-canonical ensemble, the density of mobile e_g -electrons $\langle n \rangle$ is an output of the calculation, the input being the

chemical potential μ . In Fig. 1.12(a), the density $\langle n \rangle$ vs. μ is shown for one dimensional clusters of different sizes at low temperature and large Hund coupling, in part (b) results in two dimensions are presented, and in part (c) the limit $D=\infty$ is considered. In all cases, a clear *discontinuity* in the density appears at a particular value of μ , as in a first-order phase transition. This means that there is a finite range of densities which are simply unreachable, i.e., that they cannot be stabilized regardless of how carefully μ is tuned. In the inset of Fig. 1.12(a), the spin correlations are shown for the two densities at the extremes of the discontinuity, and they correspond to FM and AF states.

Strictly speaking, the presence of PS means that the model has a range of densities which cannot be accessed, and thus, those densities are simply *unstable*. This is clarified better using now the canonical ensemble, where the number of particles is fixed as an input and μ is an output. In this context, suppose that one attempts to stabilize a density such as $\langle n \rangle = 0.95$ (unstable in Fig. 1.12), by locating, say, 95 electrons into a 10×10 lattice. The ground-state of such a system will not develop a uniform density, but instead two regions separated in space will be formed: a large one with approximately 67 sites and 67 electrons (density 1.0) and a smaller one with 33 sites and 28 electrons (density ~ 0.85). The last density is the lower value in the discontinuity of Fig. 1.12(b) in 2D, i.e., the first stable density after $\langle n \rangle = 1.0$ when holes are introduced. Then, whether using canonical or grand-canonical approximations, a range of densities remains unstable.

The actual spatial separation into two macroscopic regions (FM and AF in this case) leads to an energy problem. In the simulations and other mean-field approximations that produce PS, the “tail” of the Coulomb interaction was not explicitly included. In other words, the electric charge was not properly accounted for. Once this long-range Coulomb interaction is introduced into the problem, the fact that the FM and AF states involved in PS have different densities leads to a huge energy penalization even considering a large dielectric constant due to polarization (charge certainly cannot be accumulated in a macroscopic portion of a sample). For this reason, it is more reasonable to expect that the PS domains will break into smaller pieces. The shape of these pieces remains to be investigated in detail since the calculations are difficult with long-range interactions (for results in 1D see below), but droplets or stripes appear as a serious possibility. This state would now be *stable*, since it would satisfy in part the tendency toward phase separation and also it will avoid a macroscopic charge accumulation. Although detailed calculations are not available, the common folklore is that the typical size of the clusters in the mixed-phase state arising from the competition PS

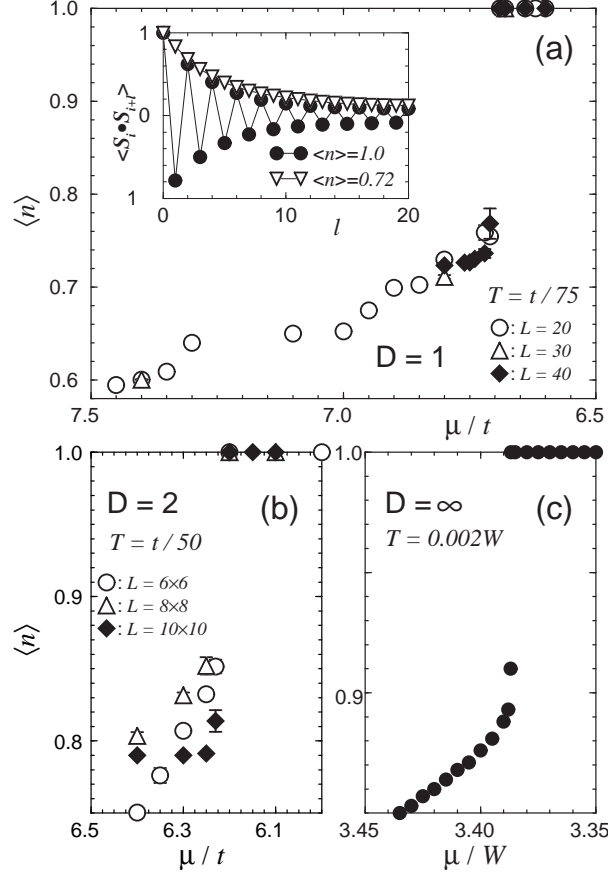


Figure 1.12. Density of e_g electrons vs chemical potential μ . The coupling is $J_H=8t$ in (a) and (b) and $4W$ in (c) (W is the half-width of the density of states). Temperatures and lattice sizes are indicated. (a) Results in 1D with PBC. The inset contains the spin correlations at the electronic densities 1.00 and 0.72, that approximately limit the density discontinuity. (b) Same as (a) but in 2D. (c) Same as (a) but in $D=\infty$. Results reproduced from Yunoki et al. (1998a).

vs. $1/r$ Coulomb will be in the *nanometer* scale, i.e., just a few lattice spacings since the Mn-Mn distance is about 4\AA . This is the electronic “Phase Separated” state that one usually has in mind as interpolating between FM and AF. Small clusters of FM are expected to be created in the AF background, and as the hole density grows, these clusters will increase in number and eventually overcome the AF clusters.

The unstable character of the low hole-density region of the phase diagram corresponding to the one-orbital model for manganites has also been analyzed by other authors using mostly analytic approximate tech-

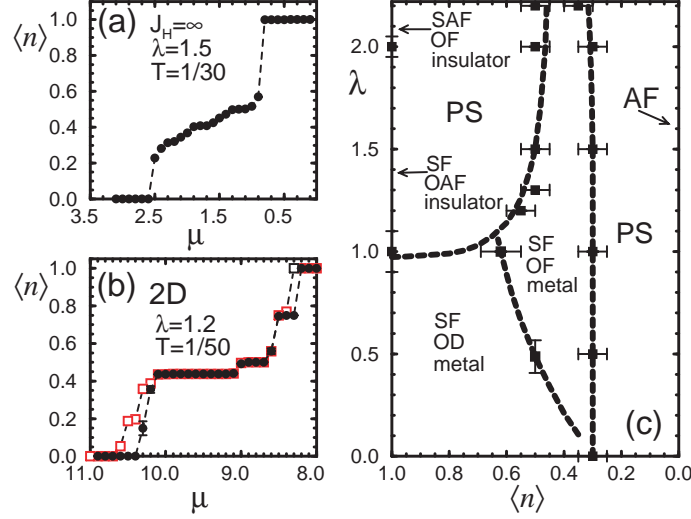


Figure 1.13. (a) $\langle n \rangle$ vs μ at the couplings and temperature indicated on a $L=22$ site chain. The discontinuities characteristic of phase separation are clearly shown. (b) Same as (a) but in 2D at the parameters indicated. The two sets of points are obtained by increasing and decreasing μ , forming a hysteresis loop. (c) Phase diagram of the two orbitals model in 1D, $J_H=8$, $J'=0.05$, and using the hopping set $t_{aa}=t_{bb}=2t_{ab}=2t_{ba}$. The notation has been explained in the text. For more details see Yunoki et al. (1998b), from where this figure was reproduced.

niques. The reader can find an extensive list of references in the review Dagotto, Hotta, and Moreo (2001) or in Dagotto (2002).

4.2 Electronic Phase Separation with Two Orbitals

Now let us analyze the phase diagram at densities away from $\langle n \rangle = 1.0$. In the case of the one-orbital model, phase separation was very prominent in this regime. In the case of the two orbitals model, discontinuities in $\langle n \rangle$ vs. μ appear similarly as for one orbital, signalling the presence of phase separation tendencies, as shown in Fig. 1.13(a) and (b). Measurements of spin and orbital correlations, as well as the Drude weight to distinguish between metallic and insulating behavior, have suggested the phase diagram in one dimension reproduced in Fig. 1.13(c). There are several phases in competition. At $\langle n \rangle = 1.0$ the results were already described in the previous subsection. Away from the $\langle n \rangle = 1.0$ phases, only the spin-FM orbital-disordered survives at finite hole density, as expected due to the mapping at small λ into the one-orbital model with half the density. The other phases at $\lambda \geq 1.0$ are not stable, but electronic

phase separation takes place. The $\langle n \rangle < 1.0$ extreme of the PS discontinuity is given by a spin-FM orbital-FM metallic state, which is a 1D precursor of the metallic orbitally-ordered A-type state identified in some compounds precisely at densities close to 0.5. Then, the two states that compete in the $\langle n \rangle \sim 1.0$ PS regime differ in their orbital arrangement, but not in the spin sector. This is PS triggered by the *orbital* degrees of freedom, which is a novel concept. On the other hand, the PS observed at low density is very similar to that observed in the one-orbital model involving spin FM and AF states in competition. Finally, at $\langle n \rangle \sim 0.5$ and large λ , charge ordering takes place, but this phase will be discussed in more detail later. Overall, it is quite reassuring to observe that the stable phases in Fig. 1.13(c) all have an analog in experiments. This gives support to the models used and to the computational and mean-field techniques employed.

In addition, since all stable regions are realistic, it is natural to assume that the rest of the phase diagram, namely the PS regions, must also have an analog in experiments in the form of mixed-phase tendencies and nanometer-size cluster formation, as discussed in the case of the one-orbital model. PS is very prominent in all the models studied, as long as proper many-body techniques are employed.

4.3 Pseudogap in Mixed-Phase States

Recent theoretical investigations suggest that the density of states (DOS) in mixed-phase regimes of manganites may have “pseudogap” characteristics, namely a prominent depletion of weight at the chemical potential. This feature is similar to that extensively discussed in copper oxides. The calculations in the Mn-oxide context have been carried out using both the one- and two-orbital models, with and without disorder (see Moreo, Yunoki and Dagotto, 1999b; Moreo et al., 2000). Typical results are shown in Fig. 1.14. Part (a) contains the DOS of the one-orbital model on a 2D cluster varying the electronic density slightly below $\langle n \rangle = 1.0$, as indicated in the caption. At zero temperature, this density regime is unstable due to phase separation, but at the temperature of the simulation those densities still correspond to stable states, but with a dynamical mixture of AF and FM features (as observed, for instance, in Monte Carlo snapshots of the spin configurations). A clear minimum in the DOS at the chemical potential can be observed. Very similar results appear also in 1D simulations (Moreo, Yunoki and Dagotto, 1999b). Part (b) contains results for two-orbitals and a large electron-phonon coupling, this time at a fixed density and changing temperature. Clearly a pseudogap develops in the system as a precursor of the phase separation that is reached as the temperature is further re-

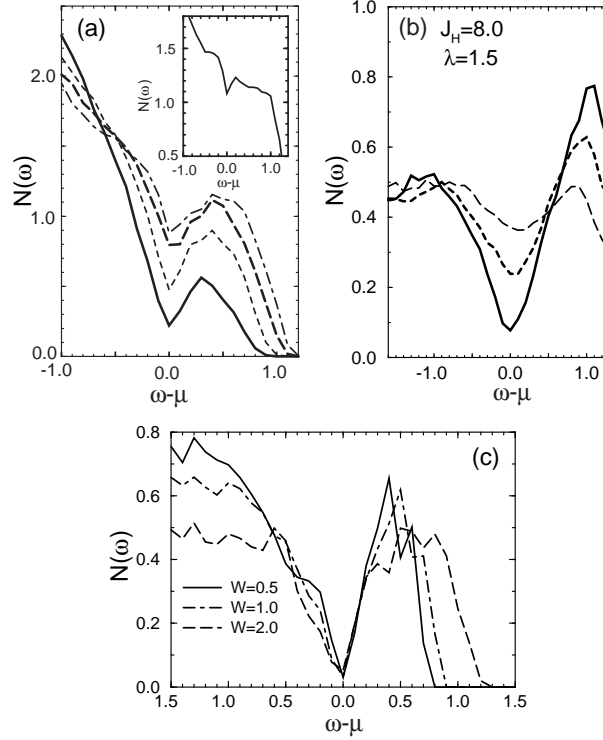


Figure 1.14. (a) DOS of the one-orbital model on a 10×10 cluster at $J_H = \infty$ and temperature $T = 1/30$ (hopping $t = 1$). The four lines from the top correspond to densities 0.90, 0.92, 0.94, and 0.97. The inset has results at $\langle n \rangle = 0.86$, a marginally stable density at $T = 0$. (b) DOS of the two-orbital model on a 20-site chain, working at $\langle n \rangle = 0.7$, $J_H = 8$, and $\lambda = 1.5$. Starting from the top at $\omega - \mu = 0$, the three lines represent temperatures $1/5$, $1/10$, and $1/20$, respectively. Here the hopping along x between orbitals a is the unit of energy. Both, (a) and (b) are taken from Moreo, Yunoki, and Dagotto (1999b). (c) DOS using a 20-site chain of the one-orbital model at $T = 1/75$, $J_H = 8$, $\langle n \rangle = 0.87$, and at a chemical potential such that the system is phase-separated in the absence of disorder. W regulates the strength of the disorder, as explained in Moreo et al. (2000) from where this figure was taken.

duced. Similar results have been obtained in other parts of parameter space, as long as the system is near unstable phase-separated regimes. Pseudogaps in the DOS appear also through the influence of disorder on first-order transitions (see Fig. 1.14(c)), issue to be discussed in the next section”.

A tentative detailed explanation of this phenomenon for the case without disorder was described by Moreo, Yunoki, and Dagotto (1999b), but intuitively it is clear that a mixture of an insulator (with a gap in the density of states) and a metal (with a featureless density of states), will

lead to an intermediate situation as it is the pseudogap. In this respect, the appearance of the pseudogap is natural when metals and insulators compete.

4.4 Phase Separation Caused by the Influence of Disorder on First-Order Transitions

Although it is frequently stated in the literature that a variety of chemical substitutions in manganites lead to modifications in the bandwidth due to changes in the “average” A-site cation radius $\langle r_A \rangle$, this statement is only partially true. Convincing analysis of data and experiments by Rodriguez-Martinez and Attfield (1996) have shown that the disorder introduced by chemical replacements in the A-sites is also crucially important in determining the properties of manganites. For instance, Rodriguez-Martinez and Attfield (1996) found that the critical temperature T_C can be reduced by a large factor if the variance σ^2 of the ionic radii about the mean $\langle r_A \rangle$ is modified, keeping $\langle r_A \rangle$ constant. Rodriguez-Martinez and Attfield (1996) actually observed that maximum magnetoresistance effects are found in materials not only with a low value of $\langle r_A \rangle$ (small bandwidth) but also a small value of σ^2 . A good example is $\text{Pr}_{1-x}\text{Ca}_x\text{MnO}_3$ since the Pr^{3+} and Ca^{2+} ions are similar in size (1.30 Å and 1.34 Å, respectively, according to Tomioka and Tokura (1999)).

Disorder, as described in the previous paragraph, is important for the phase separation scenario. The recent experimental results showing the existence of micrometer size coexisting clusters in $(\text{La}_{5/8-y}\text{Pr}_y)\text{Ca}_{3/8}\text{MnO}_3$ (LPCMO) by Uehara et al. (1999), to be reviewed in detail later, highlights a property of manganites that appears universal, namely the presence of intrinsic inhomogeneities in the system, even in single crystals. This issue is discussed at length in various sections of this review. In the theoretical framework described thus far, the scenario that is the closest to predicting such inhomogeneous state is the one based on electronic phase separation. However, the analysis presented before when considering the influence of long-range Coulomb interactions over a phase separated state, led us to believe that only nanometer size coexisting clusters are to be expected in this problem. Those found in LPCMO are much larger, suggesting that there must be another mechanism operative in manganites to account for their formation.

A possible explanation of the results of Uehara et al. (1999) has been recently proposed by Moreo et al. (2000), and it could be considered as a form of “disorder-induced” or “structural” phase separation, rather than electronic. The idea is based on the influence of disorder over the first-order metal-insulator (or FM-AF) transition found in models

where the interactions are translationally invariant (without disorder). When such a transition occurs, abruptly a metal changes into an insulator, as either concentrations or couplings are suitably changed. Unless metastable states are considered, there is no reason to assume that in the actual stable ground-state of this system coexisting clusters will be found, namely the state is entirely FM or AF depending on parameters. However, different is the situation when disorder is considered into the problem. The type of disorder taken into account by Moreo et al. (2000) is based on the influence of the different ionic radius of the various elements that compose the manganites. Depending on the environment of A-type ions (which in LPCMO involve La, Pr or Ca) a given Mn-O-Mn bond can be straight (180°) or distorted with an angle less than 180° . In the latter, the hopping across the bond under study will be less than the ideal one. The random character of the distribution of A ions, leads to a concomitant random distribution of hoppings, and also random exchange between the localized spins J_{AF} since this quantity is also influenced by the angle of the Mn-O-Mn bond.

To account for this effect, Moreo et al. (2000) studied the one- and two-orbital models for manganites described before, including a small random component to both the hoppings and J_{AF} . This small component did not influence the FM and AF phases much away from their transition boundary, but in the vicinity of the first-order transition its influence is important. In fact, numerical studies show that the transition now becomes continuous, with FM and AF clusters in coexistence in a narrow region around the original transition point.

Typical results are shown in Figs. 1.15(a)-(f), using one-dimensional clusters as an example. In the two upper frames, the energy versus J_{AF} (or J') is shown at fixed values of the other couplings such as J_H and λ , in the absence of disorder and at a fixed density $x=0.5$. The abrupt change in the slope of the curves in (a) and (d) clearly shows that the transition is indeed first-order. This is a typical result that appears recurrently in all Monte Carlo simulations of manganite models, namely FM and AF are so different that the only way to change from one to the other at low temperature is abruptly in a discontinuous transition (and spin canted phases have not been found in our analysis in the absence of magnetic fields, as possible intermediate phases between FM and AF). These results are drastically changed upon the application of disorder, as shown in frames (b,c,e, and f) of Fig. 1.15, where the mean couplings have been fixed such that the model is located exactly at the first-order transition of the non-disordered system. In these frames, the nearest-neighbor spin correlations along the chain are shown. Clearly this correlation is positive in some portions of the chain, while it alter-

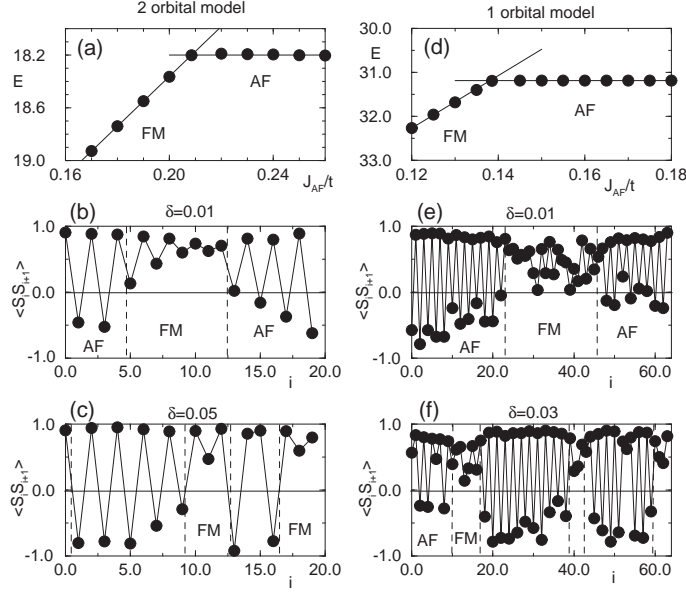


Figure 1.15. Results that illustrate the generation of “giant” coexisting clusters in models for manganites (taken from Moreo et al., 2000). (a-c) are Monte Carlo results for the two-orbital model with $\langle n \rangle = 0.5$, $T = 1/100$, $J_H = \infty$, $\lambda = 1.2$, $t = 1$, PBC, and using a chain with $L = 20$ sites. (a) is the energy per site vs J_{AF}/t for the non-disordered model, with level crossing at 0.21. (b) MC averaged nearest-neighbor t_{2g} -spins correlations vs position along the chain (denoted by i) for one set of random hoppings t_{ab}^α and J_{AF} couplings (J_{AF}/t at every site is between $0.21 - \delta$ and $0.21 + \delta$ with $\delta = 0.01$). FM and AF regions are shown. For more details see Moreo et al. (2000). (c) Same as (b) but with $\delta = 0.05$. (d-f): results for the one-orbital model with $\langle n \rangle = 0.5$, $T = 1/70$, $J_H = \infty$, $t = 1$, open boundary conditions, and $L = 64$ (chain). (d) is energy per site vs J_{AF} for the non-disordered model, showing the FM-AF states level crossing at $J_{AF} \sim 0.14$. (e) are the MC averaged nearest-neighbor t_{2g} -spin correlations vs position for one distribution of random hoppings and t_{2g} exchanges, such that J_{AF}/t is between $0.14 - \delta$ and $0.14 + \delta$ with $\delta = 0.01$. (f) Same as (e) but with $\delta = 0.03$.

mates from positive to negative in others. This alternation is compatible with an AF state, with an elementary unit cell of spins in the configuration up-up-down-down, but the particular form of the AF state is not important in the following; only its competition with other ordered states, such as the FM one is significant. The important point is that there are coexisting FM and AF regions. The cluster size is regulated by the strength of the disorder, such that the smaller the disorder, the larger the cluster size. Results such as those in Fig. 1.15 have appeared in all simulations carried out in this context, and in dimensions larger than one (see Moreo et al., 2000). The conclusions appear independent

of the particular type of AF insulating state competing with the FM state, the details of the distribution of random numbers used, and the particular type of disorder considered which could also be in the form of a random on-site energy in some cases (Moreo et al., 2000). Note that the coexisting clusters have the *same* density, namely these are FM and AF phases that appear at a fixed hole concentration in the non-disordered models, for varying couplings. Then, the problem of a large penalization due to the accumulation of charge is not present in this context.

What is the origin of such a large cluster coexistence with equal density? There are two main opposing tendencies acting in the system. On one hand, energetically it is not convenient to create FM-AF interfaces and from this perspective a fully homogeneous system is preferable. On the other hand, locally at the level of the lattice spacing the disorder in t and J_{AF} alter the couplings such that the system prefers to be either on the FM or AF phases, since these couplings fluctuate around the transition value. From the perspective of the disorder, the clusters should be as small as possible such that the local different tendencies can be properly accounted for. From this competition emerges the large clusters of Fig. 1.15, namely by creating large clusters, the number of interfaces is kept small while the local tendencies toward one phase or the other are partially satisfied. “Large” here means substantially larger in size than the lattice spacing. A region where accidentally the distribution of random couplings favors the FM or AF state on average, will nucleate such a phase in the form of a bubble.

Very recent results in this context have been presented by Burgy *et al.* (2001) where the competition of two phases was analyzed in general terms, and the resistivity was calculated with a resistor network approximation. A clearly large MR effect was observed, and extensions to cuprates were proposed.

Summarizing, phase separation can be driven by energies other than purely electronic. In fact it can also be triggered by the influence of disorder on first-order transitions. In this case the competing clusters have the same density and for this reason can be very large. Micrometer size clusters, such as those found in the RFIM, are possible in this context, and have been observed in experiments. This result is very general, and should apply to a variety of compounds where two very different ordered states are in competition at low temperatures.

4.5 Resistivity of Manganites in the Mixed-Phase Regime

One of the main lessons learned from the previous analysis of models for manganites is that intrinsic inhomogeneities are very important in this context. It is likely that the real Mn-oxides in the CMR regime are in such a mixed-phase state, a conclusion that appears inevitable based on the huge recent experimental literature, reporting phase separation tendencies in some form or another in these compounds. However, note that until recently estimations of the d.c. resistivity ρ_{dc} in such a mixed-phase regime were not available. This was unfortunate since the interesting form of the ρ_{dc} vs. temperature curves, parametric with magnetic fields, is one of the main motivations for the current huge effort in the manganite context. However, the lack of *reliable* estimations of ρ_{dc} is not accidental: it is notoriously difficult to calculate transport properties in general, and even more complicated in regions of parameter space that are expected to be microscopically inhomogeneous. Although there have been some attempts in the literature to calculate ρ_{dc} , typically a variety of approximations that are not under control have been employed. In fact, the micrometer size of some of the coexisting clusters found in experiments strongly suggest that a fully microscopic approach to the problem will likely fail since, e.g., in a computational analysis it would be very difficult to study sufficiently large clusters to account for such large scale structures. It is clear that a more phenomenological approach is needed in this context.

For all these reasons, recently a two effective resistance picture of the physics of manganites was proposed by Mayr et al. (2000). A sketch of this idea is in Fig. 1.16. Mayr et al. (2001) carried out a study of ρ_{dc} using a *random resistor network* model (see Kirkpatrick, 1973), and other approximations. This model was defined on square and cubic lattices, but with a lattice spacing much larger than the 4\AA distance between nearest-neighbor Mn ions. Actually, the new lattice spacing is a fraction of micrometer, since the random network tries to mimic the complicated fractalic-like structure found experimentally. At each link in this sort of effective lattice, randomly either a metallic or insulating resistance was located in such a way that the total fraction of metallic component was p , a number between 0 and 1.

The actual values of these resistances as a function of temperature were taken from experiments. Mayr et al. (2001) used the $\rho_{dc}(T)$ plots obtained by Uehara et al. (1999) corresponding to $(\text{La}_{5/8-y}\text{Pr}_y)\text{Ca}_{3/8}\text{MnO}_3$ (LPCMO), one of the compounds that presents the coexistence of giant FM and CO clusters at intermediate values of the Pr concentra-

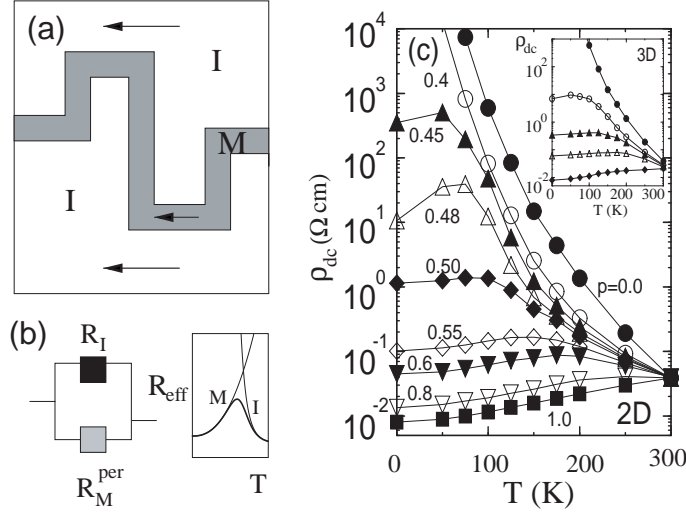


Figure 1.16. (a) Mixed-phase state near percolation. Arrows indicate conduction through insulating or metallic regions depending on T . (b) Two-resistances model for Mn-oxides. Effective resistance R_{eff} vs. T (schematic) arising from the parallel connection of metallic (percolative) R_M^{per} and insulating R_I resistances. (c) Net resistivity ρ_{dc} of a 100×100 random resistor network cluster vs temperature, at the indicated metallic fractions p (result taken from Mayr et al., 2000). Inset: Results for a 20^3 cluster with (from the top) $p=0.0, 0.25, 0.3, 0.4$ and 0.5 . In both cases, averages over 40 resistance configurations were made. The $p=1$ and 0 limits are from the experiments corresponding to LPCMO (see Uehara et al., 1999). Results on 200×200 clusters (not shown) indicate that size effects are negligible.

tion. More specifically, using for the insulating resistances the results of LPCMO at $y=0.42$ (after the system becomes a CO state with increasing Pr doping) and for the metallic ones the results at $y=0.0$ (which correspond to a metallic state, at least below its Curie temperature), the results of a numerical study on a 100×100 cluster are shown in Fig. 1.16 (the Kirchoff equations were solved by a simple iterative procedure). It is interesting to observe that, even using such a simple phenomenological model, the results are already in reasonable agreement with the experiments, namely, (i) at large temperature insulating behavior is observed even for p as large as 0.65 (note that the classical percolation is expected to occur near $p = 0.5$; see Kirkpatrick (1973)); (ii) at small temperature a (“bad”) metallic behavior appears; and (iii) a broad peak exists in between. Results in both 2D and 3D lead to similar conclusions. It is clear that the experimental results for manganites can be at least partially accounted for within the mixed-phase scenario.

The results of Fig. 1.16 suggest a simple qualitative picture to visualize why the resistivity in Mn-oxides has the peculiar shape it has. The relevant state in this context should be imagined as percolated. Metallic filaments from one side of the sample to the other exist in the system. At low temperature, conduction is through those filaments. Necessarily, ρ_{dc} at $T=0$ must be large, in such a percolative regime. As temperature increases, the ρ_{dc} of the filaments grows as in any metal. However, in the other limit of large or room temperature, the resistance of the percolated metallic filament is expected to be much larger than that corresponding to one of the insulator paths. Actually, near room temperature in many experimental graphs, it can be observed that ρ_{dc} in the metallic and insulating regimes are quite similar in value, even comparing results away from the percolative region. Then, at room temperature it is more likely that conduction will occur through the insulating portions of the sample, rather than through the metallic filaments. Thus, near room temperature insulating behavior is expected. In between low and high temperature, it is natural that ρ_{dc} will present a peak. Then, a simple “two resistances in parallel” description appears appropriate. The insulating resistance behaves like any insulator, while the metallic one starts at $T=0$ at a high value and then it behaves like any metal. The resulting effective resistance properly reproduces the experiments at least qualitatively.

The success of the phenomenological approach described above leads to an interesting prediction. In the random resistor network, it is clear that above the peak in the resistivity, the mixed-phase character of the system remains, even with a temperature dependent metallic fraction p . Then, it is conceivable to imagine that above the Curie temperature in real manganites, a substantial fraction of the system should remain in a metallic FM state (likely not percolated, but forming disconnected clusters). A large variety of experiments indeed suggest that having FM clusters above T_C is possible. As a consequence, this has led us to conjecture that there must exist a temperature T^* at which those clusters start forming. This defines a new temperature scale in the problem, somewhat similar to the famous pseudogap T^* scale of the high temperature superconducting compounds. In fact, in mixed phase FM-AF states it is known that a pseudogap appears in the density of states (Moreo et al., 1999b; Moreo et al., 2000), thus increasing the analogy between these two materials. In our opinion, the experimental verification that indeed such a new scale T^* exists in manganites is important to our understanding of these compounds. In fact, recent results by Kim, Uehara and Cheong (2000) for $\text{La}_{1-x}\text{Ca}_x\text{MnO}_3$ at various densities have been interpreted as caused by small FM segments of the CE-type CO

state, appearing at hole densities smaller than $x=1/2$ and at high temperature. This result is in qualitative agreement with the theoretical analysis presented here.

The study of effective resistivities and conductances has also been carried out in the presence of magnetic fields (Mayr et al., 2001), although still mainly within a phenomenological approach. From the previous results, it is clear that in the percolative regime “small” changes in the system may lead to large changes in the resistivity. It is conceivable that small magnetic fields could induce such small changes in p , leading to substantial modifications in the resistivity. Experiments by Parisi et al. (2001) indeed show a rapid change of the fraction of the FM phase in $\text{La}_{0.5}\text{Ca}_{0.5}\text{MnO}_3$ upon the application of magnetic fields. In addition, studies of the one-orbital model carried out in one dimension (Mayr et al., 2001) also showed that other factors may influence the large ρ_{dc} changes upon the application of external fields.

5. Concluding Remarks

In this review, a small fraction of the main results gathered in recent years in the context of theoretical studies of models for manganites have been discussed. For better information the reader should consult a more extensive review by the authors and A. Moreo (Dagotto, Hotta, and Moreo, 2001) or the recent book on manganites by Dagotto (Dagotto 2002). The main experiments that have helped clarify the physics of these interesting compounds are reviewed elsewhere in this book. Several aspects of the problem are by now widely accepted, while others still need further work to be confirmed. Intrinsic inhomogeneities exist in models and experiments and seem to play a key role in these compounds.

Among the issues related with inhomogeneities that after a considerable effort appear well-established are the following:

- (1) Work carried out by several groups using a variety of techniques have shown that electronic phase separation is a dominant feature of models for manganites, particularly in the limits of small and large hole doping. This type of phase separation leads to nanometer size coexisting clusters once the long-range Coulombic repulsion is incorporated into the models.
- (2) Working at constant density, the transitions between metallic (typically FM) and insulating (typically CO/AF) states are of **first** order at zero temperature. No counter-example has been found to this statement thus far.
- (3) A second form of phase separation has been recently discussed. It is produced by the influence of disorder on the first-order metal-insulator transitions described in the previous item. If couplings are fixed such

that one is exactly at the first-order transition in the absence of disorder, the system is “confused” and does not know whether to be metallic or insulating (at zero disorder). On the other hand, if the couplings are the same, but the strength of disorder is large in such a way that it becomes dominating, then tiny clusters of the two competing phases are formed with the lattice spacing as the typical length scale. For nonzero but weak disorder, an intermediate situation develops where fluctuations in the disorder pin either one phase or the other in large regions of space.

This form of phase separation is even more promising than the electronic one for explaining the physics of manganites for a variety of reasons: (i) it involves phases with the same density, thus there are no constraints on the size of the coexisting clusters which can be as large as a micrometer in scale, as found in experiments. (ii) The clusters are randomly distributed and have fractal shapes, leading naturally to **percolative** transitions from one competing phase to the other, as couplings or densities are varied. This is in agreement with many experiments that have reported percolative features in manganites. (iii) The resistivity obtained in this context is similar to that found in experiments. Near the critical amount of metallic fraction for percolation, at room temperature the charge conduction can occur through the insulating regions since their resistivity at that temperature is very similar to that of the metallic state. Thus, the system behaves as an insulator. However, at low temperatures, the insulator regions have a huge resistivity and, thus, conduction is through the percolative metallic filaments which have a large intrinsic resistivity. The system behaves as a bad metal, and $\rho_{\text{dc}}(T = 0)$ can be very large. (iv) Finally, it is expected that in a percolative regime there must be a high sensitivity to magnetic fields and other naively “small” perturbations, since tiny changes in the metallic fraction can induce large conductivity modifications. This provides the best explanation of the CMR effect of which these authors are aware.

(4) The experimental evidence for inhomogeneities in manganites is by now simply overwhelming. Dozens of groups, using a variety of techniques, have converged to such a conclusion. It is clear that homogeneous descriptions of manganites in the region of interest for the CMR effect are incorrect. These inhomogeneities appear even above the Curie temperature. In fact, the present authors believe that a new scale of temperature T^* should be introduced (see Burgy et al., 2001). There must be a temperature window where coexisting clusters exist above the temperatures where truly long-range order develops. Part of the clusters can be metallic, and their percolation may induce long-range order as temperature decreases. The region below T^* can be as interesting

as that observed in high temperature superconductors, at temperatures higher than the critical values. It is likely that it contains pseudogap characteristics, due to its low conductivity in low bandwidth manganites. The search for a characterization of T^* should be pursued actively in experiments.

(5) The famous CE-state of half-doped manganites has been shown to be stable in mean-field and computational studies of models for manganites. Although such a state was postulated a long time ago, it is only recently that it has emerged from unbiased studies. The simplest view to understand the CE-state is based on a “band insulating” picture: it has been shown that in a zigzag FM chain a gap opens at $x=0.5$, reducing the energy compared with straight chains. Thus, elegant geometrical arguments are by now available to understand the origin of the naively quite complicated CE-state of manganites. Its stabilization can be rationalized based simply on models of non-interacting spinless fermions in 1D geometries. In addition, theoretical studies have allowed one to analyze the properties of the states competing with the CE at $x=0.5$. In order to arrive at the CE-state, the use of a strong long-range Coulomb interaction to induce the staggered charge pattern is not correct, since by this procedure the experimentally observed charge-stacking along the z -axis could not be reproduced, and in addition the metallic regimes at $x=0.5$ found in some manganites would not be stable. Manganese oxides are in the subtle regime where many different tendencies are in competition.

(6) Contrary to what was naively believed until recently, studies with strong electron Jahn-Teller phonon coupling or with strong on-site Coulomb interactions lead to quite similar phase diagrams. The reason is that both interactions disfavor double occupancy of a given orbital. Thus, if the goal is to understand the CMR effect, the important issue is not whether the material is Jahn-Teller or Coulomb dominated, but how the metallic and insulating phases, of whatever origin, compete. Calculations with Jahn-Teller phonons are the simplest in practice, and they have led to phase diagrams that contain most of the known phases found experimentally for manganites, such as the A-type AF insulating state at $x=0$, the A-type AF metallic state at $x=0.5$, the CE-state at $x=0.5$, etc. Such an agreement theory-experiment is quite remarkable and encouraging.

(7) Also contrary to naive expectations, the smallest parameter in realistic Hamiltonians for Mn-oxides, namely “ J_{AF} ” between localized t_{2g} spins, plays an important role in stabilizing the experimentally observed phases of manganites, including the CE-state. Modifications of this coupling due to disorder are as important as those in the hopping amplitudes for e_g electron movement.

As a conclusion, it is clear that the present prevailing paradigm for manganites relies on a phase-separated view of the dominant state, as suggested by dozens of experiments and also by theoretical calculations once powerful many-body techniques are used to study realistic models.

Although considerable progress has been achieved in recent years in the analysis of manganites, both in theoretical and experimental aspects, there are still a large number of issues that require further work. Here a partial list of **open questions** is included.

(a) The phase separation scenario needs further experimental confirmation. Are there counterexamples of compounds where CMR occurs but the system appears homogeneous?

(b) On the theory front, a phase-separated percolative state is an important challenge to our computational abilities. Is it possible to produce simple formulas with a small number of parameters that experimentalists can use in order to fit their, e.g., transport data?

(c) The generation of a “Quantum Critical Point” (QCP) is likely in the context of competing phases, and preliminary results support this view (Burgý et al., 2001). Can this be observed experimentally?

(d) There is not much reliable theoretical work carried out in the presence of magnetic fields addressing directly the CMR effect.

(e) If the prediction of a phase-separated state in the CMR regime of manganites is experimentally fully confirmed, what are the differences between that state and a canonical “spin-glass”? Both share complexity and complicated time dependences, but are they in the same class? Stated in more exciting terms, can the phase-separated regime of manganites be considered a “new” state of matter in any respect?

(f) Considerable progress has been achieved in understanding the $x=0$ and $x=0.5$ charge/orbital/spin order states of manganites. But little is known about the ordered states at intermediate densities, both in theory and experiments. Are there stripes in manganites at those intermediate hole densities as recently suggested by experimental and theoretical work?

Summarizing, the study of manganites continues challenging our understanding of transition-metal-oxides. While considerable progress has been achieved in recent years, much work remains to be done. In particular, a full understanding of the famous CMR effect is still lacking, although evidence is accumulating that it may be caused by intrinsic tendencies toward inhomogeneities in Mn-oxides and other compounds. Work in this challenging area of research should continue at its present fast pace.

Acknowledgement

The authors would like to thank C. Buhler, J. Burgy, S. Capponi, A. Feiguin, N. Furukawa, K. Hallberg, J. Hu, H. Koizumi, A. Malvezzi, M. Mayr, D. Poilblanc, J. Riera, Y. Takada, J. A. Verges, and S. Yunoki for valuable collaborations on manganites. E. D. was supported by NSF grant DMR-0122523. T.H. was supported by the Grant-in-Aid for Encouragement of Young Scientists from the Ministry of Education, Science, Sports, and Culture (ESSC). He has been also supported by the Grant-in-Aid for Scientific Research Priority Area from ESSC and for Scientific Research from Japan Society for the Promotion of Science.

References

- C. P. Adams, J. W. Lynn, Y. M. Mukovskii, A. A. Arsenov, and D. A. Shulyatev, Phys. Rev. Lett. **85**, 2553 (2000).
- P. B. Allen and V. Perebeinos, Phys. Rev. B **60**, 10747 (1999).
- J. L. Alonso, L. A. Fernández, F. Guinea, V. Laliena, and V. Martín-Mayor, 2001a, Phys. Rev. B **63**, 64416 (2001).
- J. L. Alonso, L. A. Fernández, F. Guinea, V. Laliena, and V. Martín-Mayor, 2001b, Phys. Rev. B **63**, 054411 (2001).
- J. L. Alonso, L. A. Fernández, F. Guinea, V. Laliena, and V. Martín-Mayor, 2001c, Nucl. Phys. B **596**, 587 (2001).
- P. W. Anderson and H. Hasegawa, Phys. Rev. **100**, 675 (1955).
- V. I. Anisimov, I. S. Elfimov, M. A. Korotin, and K. Terakura, Phys. Rev. B **55**, 15494 (1997).
- T. Arima, Y. Tokura, and J. B. Torrance, Phys. Rev. B **48**, 17006 (1993).
- P. Benedetti and R. Zeyher, Phys. Rev. B **59**, 9923 (1999).
- J. J. Betouras and S. Fujimoto, Phys. Rev. B **59**, 529 (1999).
- A. Bocquet, T. Mizokawa, T. Saitoh, H. Namatame, and A. Fujimori, Phys. Rev. B **46**, 3771 (1992).
- M. Braden, G. André, S. Nakatsuji, and Y. Maeno, Phys. Rev. B **58**, 847 (1998).
- C. Buhler, S. Yunoki and A. Moreo, Phys. Rev. Lett. **84**, 2690 (2000).
- J. Burgy, M. Mayr, V. Martin-Mayor, A. Moreo, and E. Dagotto, Phys. Rev. Lett. **87**, 277202 (2001).
- M. Capone, D. Feinberg, and M. Grilli, Euro. Phys. J. B **17**, 103 (2000).

- C. Castellani, C. R. Natoli, and J. Ranninger, Phys. Rev. **18**, 4945 (1978).
- E. Dagotto, Rev. Mod. Phys. **66**, 763 (1994).
- E. Dagotto, S. Yunoki, A. L. Malvezzi, A. Moreo, J. Hu, S. Capponi, D. Poilblanc, and N. Furukawa, Phys. Rev. B **58**, 6414 (1998).
- E. Dagotto, T. Hotta, and A. Moreo, Phys. Rep. **344**, 1 (2001).
- E. Dagotto, *Nanoscale Phase Separation and Colossal Magnetoresistance*, Springer-Verlag, Berlin, 2002.
- P. Dai, J. A. Fernandez-Baca, N. Wakabayashi, E. W. Plummer, Y. Tomioka, and Y. Tokura, Phys. Rev. Lett. **85**, 2553 (2000).
- V. Emery, S. Kivelson, and H. Lin, Phys. Rev. Lett. **64**, 475 (1990).
- P. G. de Gennes, Phys. Rev. **118**, 141 (1960).
- D. S. Dessau, T. Saitoh, C.-H. Park, Z.-X. Shen, P. Villella, N. Hamada, Y. Moritomo, and Y. Tokura, Phys. Rev. Lett. **81**, 192 (1998).
- D. S. Dessau and Z.-X. Shen, Chap. 5, *Colossal Magnetoresistance Oxides*, edited by Y. Tokura, Gordon & Breach, New York, 1999.
- L. Dworin and A. Narath, Phys. Rev. Lett. **25**, 1287 (1970).
- R. Frésard and G. Kotliar, Phys. Rev. B **56**, 12909 (1997).
- N. Furukawa, J. Phys. Soc. Jpn. **63**, 3214 (1994).
- M. Gerloch and R. C. Slade, *Ligand-Field Parameters*, Cambridge, London, 1973.
- J. Goodenough, Phys. Rev. **100**, 564 (1955).
- J. S. Griffith, *The Theory of Transition-Metal Ions*, Cambridge, London, 1961.
- T. Hotta, Y. Takada, and H. Koizumi, Int. J. Mod. Phys. B **12**, 3437 (1998).
- T. Hotta, S. Yunoki, M. Mayr, and E. Dagotto, Phys. Rev. B **60**, R15009 (1999).
- T. Hotta, Y. Takada, H. Koizumi, and E. Dagotto, Phys. Rev. Lett. **84**, 2477 (2000).
- T. Hotta and E. Dagotto, Phys. Rev. B **61**, R11879 (2000).
- T. Hotta, A. Malvezzi, and E. Dagotto, Phys. Rev. B **62**, 9432 (2000).
- T. Hotta, A. Feiguin, and E. Dagotto, Phys. Rev. Lett. **86**, 4922 (2001).

- T. Hotta and E. Dagotto, Phys. Rev. Lett. **88**, 017201 (2002).
- M. N. Iliev, M. V. Abrashev, H.-G. Lee, Y. Y. Sun, C. Thomsen, R. L. Meng, and C. W. Chu, Phys. Rev. B **57**, 2872 (1998).
- S. Ishihara, J. Inoue, and S. Maekawa, Phys. Rev. B **55**, 8280 (1997).
- G. Jackeli, N. B. Perkins, and N. M. Plakida, Phys. Rev. B **62**, 372 (2000).
- H. A. Jahn and E. Teller, Proc. Roy. Soc. London A **161**, 220 (1937).
- R. Kajimoto, H. Yoshizawa, H. Kawano, H. Kuwahara, Y. Tokura, K. Ohoyama, and M. Ohashi, Phys. Rev. B **60**, 9506 (1999).
- J. Kanamori, J. Appl. Phys. Suppl. **31**, 14S (1960).
- J. Kanamori, Prog. Theor. Phys. **30**, 275 (1963).
- K. H. Kim, M. Uehara, and S-W. Cheong, Phys. Rev. B **62**, R11945 (2000).
- S. Kirkpatrick, Rev. Mod. Phys. **45**, 574 (1973).
- H. Koizumi, T. Hotta, Y. Takada, 1998a, Phys. Rev. Lett. **80**, 4518 (1998).
- H. Koizumi, T. Hotta, Y. Takada, 1998b, Phys. Rev. Lett. **81**, 3803 (1998).
- W. Koshibae, Y. Kawamura, S. Ishihara, S. Okamoto, J. Inoue, and S. Maekawa, J. Phys. Soc. Jpn. **66**, 957 (1997).
- M. Korotin, T. Fujiwara, and V. Anisimov, Phys. Rev. B **62**, 5696 (2000).
- M. Kubota, Y. Oohara, H. Yoshizawa, H. Fujioka, K. Shimizu, K. Hirota, Y. Moritomo, and Y. Endoh, J. Phys. Soc. Jpn. **69**, 1986 (2000).
- K. I. Kugel and D. I. Khomskii, Sov. Phys.-JETP **37**, 725 (1974).
- J. D. Lee and B. I. Min, Phys. Rev. B **55**, R14713 (1997).
- A. Machida, Y. Moritomo, and A. Nakamura, Phys. Rev. B **58**, R4281 (1998).
- Y. Maeno, T. M. Rice, and M. Sigrist, Physics Today **54**, 42 (2001).
- R. Maezono, S. Ishihara, and N. Nagaosa, Phys. Rev. B **58**, 11583 (1998).
- R. Maezono and N. Nagaosa, Phys. Rev. B **62**, 11576 (2000).
- R. Mathieu, P. Svedlindh, and P. Nordblad, Europhys. Lett. **52** 441 (2000).

- M. Mayr, A. Moreo, J. Vergés, J. Arispe, A. Feiguin, and E. Dagotto, *Phys. Rev. Lett.* **86**, 135 (2001).
- A. Millis, B. I. Shraiman, and P. B. Littlewood, *Phys. Rev. Lett.* **74**, 5144 (1995).
- A. J. Millis, B. I. Shraiman, and R. Mueller, *Phys. Rev. Lett.* **77**, 175 (1996).
- A. J. Millis, R. Mueller, and B. I. Shraiman, *Phys. Rev.* **B54**, 5405 (1996).
- A. J. Millis, *Nature* **392**, 147 (1998).
- A. J. Millis, *Phys. Rev. Lett.* **80**, 4358 (1998).
- T. Mizokawa and A. Fujimori, *Phys. Rev.* **B51**, R12880 (1995).
- T. Mizokawa and A. Fujimori, *Phys. Rev.* **B54**, 5368 (1996).
- T. Mizokawa and A. Fujimori, *Phys. Rev.* **B56**, R493 (1997).
- T. Mizokawa, D. I. Khomskii, and G. A. Sawatzky, *Phys. Rev.* **B61**, R3776 (2000).
- T. Mizokawa, L. H. Tjeng, G. A. Sawatzky, G. Ghiringhelli, O. Tjernberg, N. B. Brookes, H. Fukazawa, S. Nakatsuji, and Y. Maeno, *Phys. Rev. Lett.* **87**, 077202 (2001).
- A. Moreo, S. Yunoki and E. Dagotto, 1999a, *Science* **283**, 2034 (1999).
- A. Moreo, S. Yunoki, and E. Dagotto, 1999b, *Phys. Rev. Lett.* **83**, 2773 (1999).
- A. Moreo, M. Mayr, A. Feiguin, S. Yunoki and E. Dagotto, *Phys. Rev. Lett.* **84**, 5568 (2000).
- S. Mori, C. H. Chen, and S.-W. Cheong, 1998a, *Nature* **392**, 473 (1998).
- S. Mori, C. H. Chen, and S.-W. Cheong, 1998b, *Phys. Rev. Lett.* **81**, 3972 (1998).
- Y. Moritomo, Y. Tomioka, A. Asamitsu, Y. Tokura, and Y. Matsui, *Phys. Rev.* **B51**, 3297 (1995).
- Y. Motome and N. Furukawa, *J. Phys. Soc. Jpn.* **68**, 3853 (1999).
- Y. Motome and N. Furukawa, *J. Phys. Soc. Jpn.* **69**, 3785 (2000).
- E. Müller-Hartmann and E. Dagotto, *Phys. Rev.* **B54**, R6819 (1996).
- S. Nakatsuji and Y. Maeno, *Phys. Rev. Lett.* **84**, 2666 (2000).
- Y. Okimoto, T. Katsufuji, T. Ishikawa, A. Urushibara, T. Arima, and Y. Tokura, *Phys. Rev. Lett.* **75**, 109 (1995).

- F. Parisi, P. Levy, G. Polla, and D. Vega, Phys. Rev. **B63**, 144419 (2001).
- J.-H. Park, C. T. Chen, S.-W. Cheong, W. Bao, G. Meigs, V. Chakarian, and Y. U. Idzerda, Phys. Rev. Lett. **76**, 4215 (1996).
- T. G. Perring, G. Aeppli, Y. Tokura, Phys. Rev. Lett. **80**, 4359 (1998).
- W. H. Press, S. A. Teukolsky, W. T. Vetterling, and B. P. Flannery, *Numerical Recipes*, Cambridge University Press, New York, 1986.
- M. Quijada, J. Cerne, J. R. Simpson, H. D. Drew, K. H. Ahn, A. J. Millis, R. Shreekala, R. Ramesh, M. Rajeswari, and T. Venkatesan, Phys. Rev. **B58**, 16093 (1998).
- P. G. Radaelli, D. E. Cox, L. Capogna, S.-W. Cheong, and M. Marezio, Phys. Rev. **B59**, 14440 (1999).
- L. M. Rodriguez-Martinez and J. P. Attfield, Phys. Rev. **B54**, R15622 (1996).
- T. Saitoh, A. Bocquet, T. Mizokawa, H. Namatame, A. Fujimori, M. Abbate, Y. Takeda, and M. Takano, Phys. Rev. **B51**, 13942 (1995).
- S. Satpathy, Z. S. Popovic, and F. R. Vukajlovic, Phys. Rev. Lett. **76**, 960 (1996).
- J. C. Slater and G. F. Koster, Phys. Rev. **94**, 1498 (1954).
- I. Solovyev, N. Hamada, and K. Terakura, Phys. Rev. Lett. **76**, 4825 (1996).
- H. Tang, M. Plihal, and D. L. Mills, J. Magn. Magn. Mat. **187**, 23 (1998).
- Y. Tokura, Chap. 1 of *Colossal Magnetoresistance Oxides*, edited by Y. Tokura, Gordon & Breach, New York, 2000.
- Y. Tomioka and Y. Tokura, Chap. 8, *Colossal Magnetoresistance Oxides*, edited by Y. Tokura, Gordon & Breach, New York, 2000.
- J. M. Tranquada, B. J. Sternlieb, J. D. Axe, Y. Nakamura, and S. Uchida, Nature **375**, 561 (1995).
- M. Uehara, S. Mori, C. H. Chen, and S.-W. Cheong, Nature **399**, 560 (1999).
- J. van den Brink, G. Khaliullin, and D. Khomskii, Phys. Rev. Lett. **83**, 5118 (1999).
- J. van den Brink, P. Horsch, F. Mack, and A. M. Oleś, Phys. Rev. **B59**, 6795 (1999).

- J. van den Brink and D. Khomskii, Phys. Rev. B **63**, R140416 (2001)
- L. Vasiliu-Doloc, S. Rosenkranz, R. Osborn, S. K. Sinha, J. W. Lynn, J. Mesot, O. H. Seeck, G. Preosti, A. J. Fedro, and J. F. Mitchell, Phys. Rev. Lett. **83**, 4393 (1999).
- E. O. Wollan and W. C. Koehler, Phys. Rev. **100**, 545 (1955).
- H. Yi, J. Yu, and S.-I. Lee, Phys. Rev. B **61**, 428 (2000)
- K. Yoshida, *Theory of Magnetism*, Springer-Verlag, Berlin, 1996.
- S. Yunoki, J. Hu, A. Malvezzi, A. Moreo, N. Furukawa, and E. Dagotto, 1998a, Phys. Rev. Lett. **80**, 845.
- S. Yunoki, A. Moreo, and E. Dagotto, 1998b, Phys. Rev. Lett. **81**, 5612.
- S. Yunoki, T. Hotta, and E. Dagotto, Phys. Rev. Lett. **84**, 3714 (2000).
- C. Zener, 1951, Phys. Rev. **82**, 403 (1951).